



UNIVERSITI PUTRA MALAYSIA

***SYNTHESIS AND CHARACTERIZATION OF LOW DIMENSIONAL AND
HETEROSTRUCTURE MAGNETIC QUANTUM AND NANOSTRUCTURE
MATERIALS PREPARED USING ELECTRODEPOSITION METHOD***

GHAZALEH BAHMAN ROKH

ITMA 2016 17



**SYNTHESIS AND CHARACTERIZATION OF LOW DIMENSIONAL AND
HETEROSTRUCTURE MAGNETIC QUANTUM AND NANOSTRUCTURE
MATERIALS PREPARED USING ELECTRODEPOSITION METHOD**

By

GHAZALEH BAHMAN ROKH

**Thesis Submitted to the School of Graduate Studies, Universiti Putra Malaysia,
in Fulfillment of the Requirements for the Degree of Doctor of Philosophy**

November 2016

COPYRIGHT

All material contained within the thesis, including without limitation text, logos, icons, photographs and all other artwork, is copyright material of Universiti Putra Malaysia unless otherwise stated. Use may be made of any material contained within the thesis for non-commercial purposes from the copyright holder. Commercial use of material may only be made with the express, prior, written permission of Universiti Putra Malaysia.

Copyright © Universiti Putra Malaysia



Abstract of thesis presented to the Senate of Universiti Putra Malaysia, in fulfillment of the Requirement for the degree of Doctor of Philosophy

SYNTHESIS AND CHARACTERIZATION OF LOW DIMENSIONAL AND HETEROSTRUCTURE MAGNETIC QUANTUM AND NANOSTRUCTURE MATERIALS PREPARED USING ELECTRODEPOSITION METHOD

By

GHAZALEH BAHMAN ROKH

November 2016

Chairman: Associate Professor Mansor Hashim, PhD
Faculty: Institute of Advanced Technology

Low dimensional structures such as nanowires, thin films and hetrostructures have attracted considerable attraction in advanced electronic devices since they exhibit diverse and interesting physical phenomena compared with bulk structures. One of the most rapidly growing fields in electronics is spintronics which combines both the spin and charge of the electrons. Compared with conventional semiconductors, dilute magnetic semiconductors (DMSs) offer better performance for new generation devices. For this purpose, group II-VI semiconductors of ZnSe and ZnS and dilute magnetic semiconductors of (Zn,Mn)Se and (Zn,Mn)S were chosen as the materials in this research. The incorporation of magnetic manganese ions in semiconductor ZnSe and ZnS structures was the source of spin-polarized electrons.

Highly technological low dimensional systems are fabricated by expensive and sophisticated methods such as molecular beam epitaxy. The problem is that the synthesis method for fabrication of such structures is very expensive. Our main attempt is to solve this problem by applying inexpensive and easy synthesis method like electrodeposition for preparation of low dimensional and heterostructures. The properties of thin films, heterostructures and nanowires were studied by applying various characterization methods.

The XRD results showed formation of highly crystallined ZnSe and ZnS thin films and the crystallinity increased at lower deposition temperatures. All deposited thin films showed mixed cubic a hexagonal structures. XRD results of Mn doped ZnSe and ZnS thin films indicated well doped samples that perfectly matched with $Zn_{1-x}Mn_xSe$ and $Zn_{1-x}Mn_xS$ ($x = 0.01, 0.05$ and 0.1). The calculated strain and dislocation density from XRD data showed a gradual increase with increasing manganese concentration. FESEM images showed that films cover perfectly the surface of ITO substrate. In addition no defects or cracks were observed on the surface of the thin films. The optical measuremets indicated that with increasing grain size and film thickness the absorption edge shifted to higher wavelengths and a red shift is observed in bandgap. The grain size and film thickness were increased

with increasing deposition temperature and deposition time. Mn doped thin films revealed a red shift with increasing manganese concentration. Very high bandgap for both semiconductor and dilute magnetic semiconductors were obtained and the bandgap blue shifted compared with bulk ZnSe and ZnS. Photoluminescence spectra for semiconductor and DMS thin films were obtained and the results showed a characteristic strong green emission peak centred at 440 nm (2.82 eV) for ZnSe. Mn-doped ZnSe systems showed a dominant yellow/orange emission present at 599 nm which results from the ${}^4T_1-{}^6A_1$ transition of the Mn^{2+} impurity excited by energy transfer from the host ZnSe lattice. The blue emission at 376 nm (3.28 eV) is obtained for ZnS thin films that attributed to surface states. The non-ohmic I-V characteristic was observed for ZnSe and ZnSe-Mn thin films. With increasing Mn concentration in ZnSe thin films the resistivity decreased. In addition the resistivity decreased with increasing the film thickness. Moreover, ZnS and ZnS thin films doped with Mn revealed ohmic behaviour. In ZnS thin films the resistivity increased as the film thickness increased. More doping leads to higher conductivity in ZnS-Mn thin films.

Single quantum well ZnSe/(Zn,Mn)Se and ZnS/(Zn,Mn)S heterostructures prepared by electrodeposition method. The thickness of quantum wells increased with increasing the deposition time. The variation in bandgap between the layers of heterostructures is investigated. The bandgap differences between barrier and quantum well materials were in the range of 100-300 meV. The quantum mechanical tunnelling and transport properties were investigated by photoluminescence, 2-point probe and electron spin resonance data. The amount of tunnelling and spin transport strongly depended on the quantum well thickness as well as the concentration of Mn in the barrier.

ZnSe, ZnS and Mn doped nanowires embedded in polycarbonate membranes revealed an increase in optical and electrical properties with decreasing the pore diameter. The higher bandgap was obtained in nanowires with smaller diameters. In addition the bandgap enhanced with increasing Mn concentration in nanowires. High resistivity and low conductivity was observed for nanowires with larger diameters.

Abstrak tesis yang dikemukakan kepada Senat Universiti Putra Malaysia sebagai memenuhi keperluan untuk ijazah Doktor Falsafah

**SINTESIS DAN PENCIRIAN KUATUM MAGNET BERDIMENSI RENDAH
DAN STRUKTUR HETERO KUANTUM MAGNET DAN BAHAN
STRUKTUR NANO YANG DISEDIAKAN DENGAN MENGGUNAKAN
TEKNIK PENGELEKTROENAPAN**

Oleh

GHAZALEH BAHMAN ROKH

November 2016

Pengerusi: Profesor Madya Mansor Hashim, PhD
Fakulti : Institut Teknologi Maju

Struktur dimensi rendah seperti nanowayar, filem nipis dan struktur hetero telah menarik tarikan yang besar dalam peralatan elektronik canggih kerana mereka mempamerkan fenomena fizikal yang pelbagai dan menarik berbanding dengan struktur pukal. Salah satu bidang yang paling pesat berkembang dalam elektronik adalah spintronik yang menggabungkan kedua-dua spin dan caj elektron. Berbanding dengan semikonduktor konvensional, semikonduktor magnet cair menawarkan prestasi yang lebih baik untuk peranti generasi baru. Untuk tujuan ini, semikonduktor Kumpulan II-VI yang terdiri dari ZnSe, ZnS semikonduktor magnet cair (Zn, Mn)Se dan (Zn, Mn)S telah dipilih sebagai bahan dalam kajian ini. Penggabungan ion mangan magnet semikonduktor dalam ZnSe dan ZnS adalah sumber sistem electron spin-terkutup. Sistem dimensi rendah berteknologi tinggi adalah difabrikasi dengan kaedah mahal dan canggih seperti epetaksi alur molekul. Usaha utama kami adalah untuk menyelesaikan masalah ini dengan menggunakan kaedah sintesis murah dan mudah seperti pengelektroenapan untuk penyediaan struktur dimensi rendah dan struktur hetero. Sifat-sifat filem nipis, struktur hetero dan wayar nano telah dikaji dengan menggunakan pelbagai kaedah pencirian.

Keputusan XRD menunjukkan pembentukan kristal ZnSe yang sangat jita dan filem nipis ZnS yang penghablurannya meningkat pada suhu pemendapan yang lebih rendah. Semua filem nipis yang didepositkan menunjukkan struktur heksagon bercampur. Keputusan XRD untuk Mn ZnSe yang didopkan Mn dan filem nipis ZnS menunjukkan pendopan sampel yang sempurna dipadankan dengan $Zn_{1-x}Mn_xSe$ dan $Zn_{1-x}Mn_xS$ ($x = 0.01, 0.05$ dan 0.1). Terikan (ϵ) yang dikira dan ketumpatan kehelan (δ) dikiradari data XRD menunjukkan peningkatan beransur-ansur dengan meningkatnya kepekatan mangan. Imej FESEM menunjukkan bahawa filem menutup dengan sempurna permukaan substrat ITO. Disamping itu tiada kecacatan atau keretakan diperhatikan pada permukaan filem nipis. Pengukuran optik menunjukkan bahawa dengan meningkatnya saiz butiran dan ketebalan filem pinggir penyerapan taranjak kearah panjang gelombang yang lebih tinggi dan anjakan merah

dicerap di dalam jurang jalur. Saiz butiran dan ketebalan filem telah meningkat dengan peningkatan suhu pemendapan dan tempoh pemendapan. Mn didopkan filem nipis mendedahkan anjakan merah dengan meningkatkan kepekatan mangan. Nilai jurang yang sangat tinggi untuk kedua-dua semikonduktor dan DMSs diperolehi dan memberikan nilai jurang anjakan biru berbanding ZnSe pukal dan ZnS. Spektrum fotoluminisen untuk filem semikonduktor dan DMS nipis diperolehi dan keputusan menunjukkan pencirian puncak pelepasan hijau yang kuat berpusat pada 440 nm (2.82 eV) untuk ZnSe. Sistem Mn-didopkan ZnSe menunjukkan dominan kuning / oren pelepasan hadir pada 599 nm yang terhasil daripada peralihan ${}^4T_1-{}^6A_1$ bendasing Mn^{2+} yang teruja dengan pemindahan tenaga dari kekisi tuan ZnSe. Pelepasan biru pada 376 nm (3.28 eV) diperolehi untuk ZnS filem nipis disebabkan oleh keadaan permukaan juga. Ciri I-V bukan ohm diperhatikan untuk ZnSe dan ZnSe-Mn filem nipis. Dengan meningkatkan kepekatan Mn dalam filem nipis ZnSe kerintangan menurun. Di samping itu kerintangan menurun dengan peningkatan tebal filem. Selain itu, ZnS dan ZnS filem nipis didopkan dengan Mn mendedahkan tingkah laku ohm. Dalam filem nipis ZnS kerintangan meningkat apabila ketebalan filem meningkat. Lebih pengedapan membawa kepada kekonduksian tinggi dalam ZnS-Mn nipis films.

Telaga tunggal kuantum ZnSe/ (Zn,Mn)Se dan struktur hetero ZnS/(Zn,Mn) disediakan dengan kaedah pegenapan. Ketebalan telaga kuantum meningkat dengan peningkatan masa pemendapan. Perubahan dalam memberikan nilai jurang antara lapisan struktur hetero disiasat. Perbezaan nilai jurang antara halangan dan telaga kuantum adalah dalam lingkungan 100-300 meV. Terowong kuantum mekanik ini dan sifat-sifat pengangkutan mekanik kuantum telah disiasat oleh data fotoluminisen, prob 2-poin dan elektron spin resonans. Jumlah terowong dan pengangkutan spin amat bergantung kepada ketebalan telaga kuantum dan juga kepekatan Mn dalam halangan. Wayar nano didopkan ZnSe, ZnS dan Mn tertanam dalam membran polikarbonat mendedahkan peningkatan dalam sifat-sifat optik dan elektrik dengan mengurangkan diameter liang itu. Nilai jurang yang lebih tinggi telah diperolehi dalam wayar nano dengan diameter yang lebih kecil. Selain itu, nilai jurang dipertingkatkan dengan peningkatan kepekatan Mn dalam wayar nano. Kerintangan yang tinggi dan kekonduksian rendah diperhatikan untuk wayar nano dengan diameter yang lebih besar.

ACKNOWLEDGEMENTS

First and for most, I would like to extend my deepest praise to Allah who has given me the patience, strength, purpose and courage to complete this project by his mercies I also would like to thank Universiti Putra Malaysia for supporting my research as international graduate research fellowship.

For the most special thanks, I would like to express my appreciation to my late proficient supervisor Associate Prof Dr Mansor Hashim who is not among us for the time I submit my thesis. God bless him and peace with his pure soul. He introduced me to the world of scientific research, and in particular to the field of magnetic nanomaterials. I have also to thank him for his guidance, suggestions and kindness which are always a strong support during my studies. I am highly indebted and extremely grateful. I would like to extend my sincere appreciation to my supervision committee members Dr Khamirul Amin Matori and Dr Lim Kean Pah, for graciously agreeing to be on my committee.

Special thanks to all my colleagues who become my best friends in the magnetic materials research group Dr Ismayadi, Shamsul, Idzah, Rodziah, Hapishah, Nora, Fazidah, Misbah, Shazwan, Hatef, Low, Eydar, Yusnita, Lyana Aizat, Dr Kanagesan. I am pleased about your hospitality, opinions and highly support especially in crucial moments. I enjoyed the memorable time we had and will have together that become a part of my life. It has been an honour to work and be with you all.

In measuring the characteristics of my sample, the efforts of Mr Rahman from UM for performing XRD, Mr Rafi from Institute of Bioscience and Mr Ali from ITMA for taking FESEM, EDX images, Ms Hanie from UKM for conducting VSM measurements are highly acknowledged. I am grateful to UPM Library which I benefited from all aspects of literature sourcing and searching.

I am highly grateful to my sister and brother; Taraneh and Shahram who always believed in me, love and supported me. I wish to thank my best and forever friends Hoda and her family, Parisa and her husband Saeed, Dr Nayereh and Manijeh, Shirin and Ghazal for all the emotional and financial support. God bless them. I owe my thanks to my extended friends, and my aunts Mahnaz and Soheila for their love and encouragement which keep me going.

Lastly and most importantly, I wish to thank my mother Shahla and to my late father Bahman for their endless love, immense patient and diligence support. Words cannot explain my love and gratitude to them. I know that I have made you proud. May his soul rest in peace and be placed amongst the blessed alongside Allah S.W.T. I couldn't have done it without you.

I attribute the level of my Doctor of Philosophy degree to all your supports. To you all I dedicate this thesis.

I certify that a Thesis Examination Committee has met on 7 November 2016 to conduct the final examination of Ghazaleh Bahman Rokh on her thesis entitled "Synthesis and Characterization of Low Dimensional and Heterostructure Magnetic Quantum and Nanostructure Materials Prepared using Electrodeposition Method" in accordance with the Universities and University Colleges Act 1971 and the Constitution of the Universiti Putra Malaysia [P.U.(A) 106] 15 March 1998. The Committee recommends that the student be awarded the Doctor of Philosophy.

Members of the Thesis Examination Committee were as follows:

Hishamuddin bin Zainuddin, PhD

Associate Professor
Faculty of Science
Universiti Putra Malaysia
(Chairman)

Abdul Halim bin Shaari, PhD

Professor
Faculty of Science
Universiti Putra Malaysia
(Internal Examiner)

Azmi bin Zakaria, PhD

Professor
Faculty of Science
Universiti Putra Malaysia
(Internal Examiner)

Gregory Kozlowski, PhD

Professor
Wright State University
United States
(External Examiner)



NOR AINI AB. SHUKOR, PhD

Professor and Deputy Dean
School of Graduate Studies
Universiti Putra Malaysia

Date: 26 January 2017

This thesis was submitted to the Senate of Universiti Putra Malaysia and has been accepted as fulfilment of the requirement for the degree of Doctor of Philosophy. The members of the Supervisory Committee were as follows:

Mansor Hashim, PhD

Associate Professor
Institute of Advanced Technology
Universiti Putra Malaysia
(Chairman)

Khamirul Amin Mantori, PhD

Associate Professor
Faculty of Science
Universiti Putra Malaysia
(Member)

Lim Kean Pah, PhD

Associate Professor
Faculty of Science
Universiti Putra Malaysia
(Member)

ROBIAH BINTI YUNUS, PhD

Professor and Dean
School of Graduate Studies
Universiti Putra Malaysia

Date:

Declaration by graduate student

I hereby confirm that:

- this thesis is my original work;
- quotations, illustrations and citations have been duly referenced;
- this thesis has not been submitted previously or concurrently for any other degree at any institutions;
- intellectual property from the thesis and copyright of thesis are fully-owned by Universiti Putra Malaysia, as according to the Universiti Putra Malaysia (Research) Rules 2012;
- written permission must be obtained from supervisor and the office of Deputy Vice-Chancellor (Research and Innovation) before thesis is published (in the form of written, printed or in electronic form) including books, journals, modules, proceeding, popular writings, seminar papers, manuscripts, posters, lecture notes, learning modules or any other materials as stated in the Universiti Putra Malaysia (Research) Rules 2012;
- there is no plagiarism or data falsification/fabrication in the thesis, and scholarly integrity is upheld as according to the Universiti Putra Malaysia (Graduate Studies) Rules 2003 (Revision 2012-2013) and the Universiti Putra Malaysia (Research) Rules 2012. The thesis has undergone plagiarism detection software.

Signature: _____ Date: _____

Name and Matric No: Ghazaleh Bahman Rokh, GS34532

Declaration by Members of Supervisory Committee

This is to confirm that:

- the research conducted and the writing of the thesis was under our supervision;
- supervision responsibilities as stated in the Universiti Putra Malaysia (Graduate Studies) Rules 2003 (Revision 2012-2013) are adhered to.

Signature: _____
Name of Chairman of
Supervisory
Committee: Mansor Hashim, PhD

Signature: _____
Name of Member of
Supervisory
Committee: Khamirul Amin Matori, PhD

Signature: _____
Name of Member of
Supervisory
Committee: Lim Kean Pah, PhD

TABLE OF CONTENTS

| | Page |
|---|-------------|
| ABSTRACT | i |
| ABSTRAK | iii |
| ACKNOWLEDGEMENTS | v |
| APPROVAL | vi |
| DECLARATION | viii |
| LIST OF TABLES | xiv |
| LIST OF FIGURES | xviii |
| LIST OF ABBREVIATIONS | xxxvii |
| CHAPTER | |
| 1 INTRODUCTION | 1 |
| 1.1 Background of the study | 1 |
| 1.2 Introduction to spintronics | 1 |
| 1.3 Choice of materials | 2 |
| 1.4 Importance of the study | 3 |
| 1.5 Problem statements | 4 |
| 1.6 Objectives of the study | 5 |
| 1.7 Outline of the thesis | 6 |
| 2 LITERATURE REVIEW | 7 |
| 2.1 Introduction | 7 |
| 2.2 An overview on materials for spintronic application | 7 |
| 2.3 Semiconductor materials | 8 |
| 2.3.1 Dilute magnetic semiconductor materials and properties | 9 |
| 2.4 Synthesis of low dimensional structures | 10 |
| 2.4.1 Thin film growth techniques | 10 |
| 2.4.2 Nanowire growth techniques | 14 |
| 2.5 Properties of semiconductor and magnetic semiconductor materials | 16 |
| 2.6 Spin-based II-VI magnetic semiconductor quantum structure devices | 21 |
| 2.7 Electrodeposition method | 24 |
| 2.7.1 Mechanism of electrodeposition | 24 |
| 2.7.2 Cyclic voltammetry | 25 |

| | | |
|----------|---|-----------|
| 2.8 | New approach from this research work | 28 |
| 3 | THEORY | 30 |
| 3.1 | Introduction | 30 |
| 3.2 | Semiconductor crystals | 30 |
| 3.2.1 | Band gap of semiconductors | 32 |
| 3.2.2 | II-VI semiconductors | 34 |
| 3.3 | Semiconductor nanocrystals | 34 |
| 3.3.1 | Density of states and dimensions of materials | 35 |
| 3.3.2 | Theory of confinement | 37 |
| 3.3.3 | Surface states | 39 |
| 3.4 | Dilute magnetic semiconductor | 39 |
| 3.4.1 | Exchange interaction between band and d-like electrons and spin-flip in DMS | 40 |
| 3.4.2 | Manganese substitution in II-VI compounds | 41 |
| 3.4.3 | Magnetic moments in manganese transition element | 42 |
| 3.5 | Quantum wells and heterostructures | 43 |
| 3.5.1 | Physics of a particle in quantum well | 43 |
| 3.5.2 | Electronic structure | 46 |
| 3.5.3 | Semiconductor band structure of heterostructures | 48 |
| 4 | METHODOLOGY | 53 |
| 4.1 | Introduction and experiment design | 53 |
| 4.2 | Materials | 56 |
| 4.3 | Sample preparation | 57 |
| 4.3.1 | Thin film fabrication | 57 |
| 4.3.2 | Heterostructure fabrication | 63 |
| 4.3.3 | Nanowire fabrication | 65 |
| 4.4 | Cyclic voltammetry and chrono amperometry measurements | 66 |
| 4.5 | Physical and structural measurements | 68 |
| 4.5.1 | X-ray diffractometry (XRD) | 69 |
| 4.5.2 | Transmission electron microscopy (TEM) | 71 |
| 4.5.3 | Field emission scanning electron microscopy (FESEM) and energy dispersive X-ray (EDX) | 72 |
| 4.5.4 | Atomic force microscopy (AFM) | 73 |
| 4.6 | Optical measurements | 74 |
| 4.6.1 | UV-Visible absorption spectroscopy | 74 |
| 4.6.2 | Photoluminescence spectroscopy (PL) | 76 |

| | | |
|----------|--|-----------|
| 4.7 | Electrical-Resistance measurement | 77 |
| 4.8 | Magnetic measurements | 79 |
| 4.8.1 | Vibrating sample magnetometer (VSM) | 80 |
| 4.8.2 | Electron spin resonance (ESR) | 81 |
| 4.9 | Accuracy of measurements | 83 |
| 5 | RESULTS AND DISCUSSION | 84 |
| 5.1 | Introduction | 84 |
| 5.2 | Thin film ZnSe and Mn doped ZnSe single layers | 84 |
| 5.2.1 | Cyclic voltammetry potentiostatic results | 84 |
| 5.2.2 | Physical and structural results | 94 |
| 5.2.3 | Optical results | 124 |
| 5.2.4 | Electrical-Resistance results | 140 |
| 5.2.5 | Magnetic results | 144 |
| 5.3 | Thin film ZnS and Mn doped ZnS single layers | 151 |
| 5.3.1 | Cyclic voltammetry potentiostatic results | 151 |
| 5.3.2 | Physical and structural results | 156 |
| 5.3.3 | Optical results | 186 |
| 5.3.4 | Electrical-Resistance results | 201 |
| 5.3.5 | Magnetic results | 203 |
| 5.4 | Heterostructure single quantum well ZnSe | 209 |
| 5.4.1 | Physical and structural results | 209 |
| 5.4.2 | Optical results | 219 |
| 5.4.3 | Electrical-Resistance results | 227 |
| 5.4.4 | ESR results | 233 |
| 5.5 | Heterostructure single quantum well ZnS | 236 |
| 5.5.1 | Physical and structural results | 236 |
| 5.5.2 | Optical results | 246 |
| 5.5.3 | Electrical-Resistance results | 253 |
| 5.5.4 | ESR results | 258 |
| 5.6 | Nanowire ZnSe and Mn doped ZnSe | 260 |
| 5.6.1 | Physical and structural results | 260 |
| 5.6.2 | UV-Visible results | 264 |
| 5.6.3 | Electrical-Resistance results | 270 |
| 5.7 | Nanowire ZnS and Mn doped ZnS | 272 |
| 5.7.1 | Physical and structural results | 272 |
| 5.7.2 | UV-Visible results | 277 |

| | | |
|----------|--|------------|
| 5.7.3 | Electrical-Resistance results | 283 |
| 6 | CONCLUSION | 286 |
| 6.1 | Conclusion | 286 |
| 6.1.1 | Summary of the main results for thin films | 286 |
| 6.1.2 | Summary of the main results for heterostructures | 289 |
| 6.1.3 | Summary of the main results for nanaowires | 291 |
| 6.2 | Suggestions for further works | 292 |
| | REFERENCES | 294 |
| | BIODATA OF STUDENT | 308 |
| | LIST OF PUBLICATIONS | 309 |

LIST OF TABLES

| Table | | Page |
|-------|---|------|
| 2.1 | Thin and thick film preparation methods (Vilarinho, 2005) | 11 |
| 2.2 | An overview on pure and Mn-doped ZnSe and ZnS low dimensional structures and heterostructures fabricated by various methods. | 23 |
| 3.1 | The electronic parameters of different crystal structures. | 31 |
| 4.1 | Precursor concentration and electroplating parameters for the deposition of ZnSe thin films. | 60 |
| 4.2 | Precursor concentration and electroplating parameters for the deposition of ZnSe-Mn thin films. | 61 |
| 4.3 | Precursor concentration and electroplating parameters for the deposition of ZnS thin films. | 62 |
| 4.4 | Precursor concentration and electroplating parameters for the deposition of ZnS-Mn thin films. | 62 |
| 4.5 | The compounds and deposition parameters used in preparation of 3-layer $Zn_{1-x}Mn_xSe/ZnSe/Zn_{1-x}Mn_xSe$ heterostructures. | 64 |
| 4.6 | The compounds and deposition parameters used in preparation of 3-layer $Zn_{1-x}Mn_xS/ZnS/Zn_{1-x}Mn_xS$ heterostructures. | 64 |
| 4.7 | Accuracy of the measurements. | 83 |
| 5.1 | Diffusion coefficient calculation for Se and Zn in ZnSe thin films. | 94 |
| 5.2 | XRD data of ZnSe films deposited at -0.6, 0.7 and -1.0 V for 30 minutes at 30 °C. | 96 |
| 5.3 | XRD data of ZnSe films deposited at 30, 50, 70 and 90 °C and deposition voltage of -0.65 V for 30 minutes. | 97 |
| 5.4 | XRD data of ZnSe-Mn 1% films deposited at 30, 50, 70 and 90 °C and deposition voltage of -0.95 V for 30 minutes. | 98 |
| 5.5 | XRD data of ZnSe-Mn 5% films deposited at 30, 50, 70 and 90 °C and deposition voltage of -0.95 V for 30 minutes. | 99 |
| 5.6 | XRD data of ZnSe-Mn 10% films deposited at 30, 50, 70 and 90 °C and deposition voltage of -0.95 V for 30 minutes. | 100 |

| | | |
|------|--|-----|
| 5.7 | Morphology and grain size of ZnSe films deposited at different temperatures. | 107 |
| 5.8 | Morphology and grain size of ZnSe films deposited at different time. | 109 |
| 5.9 | The values of ZnSe film thickness as a function of deposition time. | 111 |
| 5.10 | Morphology and grain size of ZnSe-Mn 1% films deposited at different temperatures. | 114 |
| 5.11 | Morphology and grain size of ZnSe-Mn 5% films deposited at different temperatures. | 116 |
| 5.12 | Morphology and grain size of ZnSe-Mn 10% films deposited at different temperatures. | 120 |
| 5.13 | AFM data of ZnSe thin films deposited for 5, 45 and 120 minutes. | 121 |
| 5.14 | AFM data of ZnSe-Mn thin films deposited at 30 and 70 °C for 30 minutes. | 124 |
| 5.15 | Optical bandgap data and size of ZnSe thin films deposited at different deposition bath temperatures. | 128 |
| 5.16 | Summary of magnetic data of Mn-doped ZnSe thin film deposited at 70 and 90 °C. | 148 |
| 5.17 | ESR data of ZnSe thin film doped with 1%, 5% and 10% manganese concentration deposited at 70 °C. | 150 |
| 5.18 | Diffusion coefficient calculation for S and Zn in ZnS thin films. | 156 |
| 5.19 | XRD data of ZnS films deposited using different concentrations and sources of Zn and S at -1.1 V vs Ag/AgCl at 70 °C for 30 minutes. | 158 |
| 5.20 | XRD data of ZnS films deposited at different voltages for 30 minutes at 30 °C. | 159 |
| 5.21 | XRD data of ZnS films deposited at 30, 50, 70 and 90 °C and deposition voltage of -1.1 V for 30 minutes. | 160 |
| 5.22 | XRD data of ZnS-Mn 1% films deposited at 30, 50, 70 and 90 °C and deposition voltage of -1.25 V for 30 minutes. | 162 |
| 5.23 | XRD data of ZnS-Mn 5% films deposited at 30, 50, 70 and 90 °C and deposition voltage of -1.25 V for 30 minutes. | 164 |
| 5.24 | XRD data of ZnS-Mn 10% films deposited at 30, 50, 70 and 90 °C and deposition voltage of -1.25 V for 30 minutes. | 164 |

| | | |
|------|--|-----|
| 5.25 | Average grain size and thickness of ZnS films deposited at different temperatures. | 175 |
| 5.26 | Average grain size and thickness of ZnS films deposited at different time. | 178 |
| 5.27 | Average grain size of ZnS-Mn films deposited at different temperatures. | 181 |
| 5.28 | AFM data of ZnSe-Mn thin films deposited at 30 and 70 °C for 30 minutes. | 186 |
| 5.29 | The UV-vis data of ZnS thin film deposited at different potential. | 187 |
| 5.30 | The UV-vis data of ZnS thin film deposited at different time. | 191 |
| 5.31 | Current-voltage data of ZnS thin films deposited at different time. | 202 |
| 5.32 | Summary of magnetic data of Mn-doped ZnS thin film deposited at 70 and 90 °C. | 206 |
| 5.33 | ESR data of ZnS thin film doped with 1%, 5% and 10% manganese concentration deposited at 70 °C. | 207 |
| 5.34 | XRD data of heterostructures with three different ZnSe well thicknesses. | 211 |
| 5.35 | The thickness values of quantum wells prepared with altered Mn concentrations in ZnSe-Mn barrier and different quantum well deposition time. | 219 |
| 5.36 | Bandgap energy (E_g) and the ZnSe quantum well thickness values of $Zn_{1-x}Mn_xSe/ZnSe/Zn_{1-x}Mn_xSe$ ($x = 0.01, 0.05, 0.1$) heterostructures. | 222 |
| 5.37 | Current-voltage data of ZnMnSe/ZnSe/ZnMnSe heterostructure with 1% Mn concentration and different ZnSe well thickness. | 228 |
| 5.38 | Current-voltage data of ZnMnSe/ZnSe/ZnMnSe heterostructure with 5% Mn concentration and different ZnSe well thickness. | 229 |
| 5.39 | ESR data of heterostructure ZnMnSe/ZnSe/ZnMnSe doped with 1%, 5% and 10% manganese concentration. | 233 |
| 5.40 | XRD data of heterostructures with three different ZnS well thicknesses. | 238 |
| 5.41 | The average thicknesses of the layers for the samples with different quantum well thickness, first and third layer: ZnMnS 10% quantum barrier, second layer: ZnS quantum well. | 243 |

| | | |
|------|---|-----|
| 5.42 | The thickness values of quantum wells prepared with altered Mn concentrations in ZnS-Mn barrier and different quantum well deposition time. | 246 |
| 5.43 | Bandgap energy (E_g) and the ZnS quantum well thickness values of $Zn_{1-x}Mn_xS/ZnS/Zn_{1-x}Mn_xS$ ($x = 0.01, 0.05, 0.1$) heterostructures. | 248 |
| 5.44 | Current-voltage data of ZnMnS/ZnS/ZnMnS heterostructures with different Mn concentration in the barrier and different ZnS well thicknesses. | 255 |
| 5.45 | ESR data of heterostructure ZnMnS/ZnS/ZnMnS doped with 1%, 5% and 10% manganese concentration. | 259 |
| 5.46 | UV-vis data of ZnSe and Mn-doped ZnSe nanowires. | 268 |
| 5.47 | Summary of the electrical for ZnSe nanowires doped with manganese. | 271 |
| 5.48 | UV-vis data of ZnS and Mn-doped ZnS nanowires. | 281 |
| 5.49 | The electrical data for ZnS nanowires with different pore diameter grown in PC TE. | 283 |

LIST OF FIGURES

| Figure | Page |
|---|------|
| 1.1 Summary of the energy gap at 4.2 K and lattice parameter of some II-VI MS alloys. The lines showing ternary alloys (Awschalom and Samarth, 1999). | 4 |
| 2.1 Morphology of some 1D nanostructures; A) nanowires, B) nanorods, C) nanotubes, D) nanobelts, E) nanoribbons and F) hierarchical (Chen, <i>et al.</i> , 2015a). | 10 |
| 2.2 Schematic view of an MBE growth chamber (Eaton, <i>et al.</i> , 2015). | 13 |
| 2.3 ZnSe thin films deposited by ED a) the effect of deposition voltage on crystallinity of thin film and b) the effect of deposition time on thickness (Mahalingam, <i>et al.</i> , 2006). | 17 |
| 2.4 XRD patterns of ZnS thin film grown at different deposition temperature and the variation of bandgap (Hennayaka and Lee, 2013). | 18 |
| 2.5 The optical bandgap and electrical resistivity and conductivity of ZnS thin films doped with Mn with different thickness (Ozutok, <i>et al.</i> , 2012). | 18 |
| 2.6 XRD pattern of cubic (C) and wurtzite (X) phase of ZnS annealed at 250 °C for 1 hour. S1, S2, S3 and S4 corresponds the samples prepared at PH=4, PH=8, PH=10 and PH=12 respectively (Venkatachalam, <i>et al.</i> , 2005). | 19 |
| 2.7 XRD data of ZnSe thin film prepared by MOCVD (Seo, <i>et al.</i> , 2006). | 19 |
| 2.8 Absorption and PL spectrum of ZnSe thin film (Bakiyaraj and Dhanasekaran, 2013). | 20 |
| 2.9 a) SEM and b) TEM images of ZnSe nanowire grown by MBE (Wu, <i>et al.</i> , 2004) | 20 |
| 2.10 Band alignment of different MS heterostructures a) single quantum well; b) magnetically coupled double quantum well; c) digital magnetic heterostructure; d) two dimensional electron gas; e) type-II magnetic quantum well structure (Awschalom and Samarth, 1999). | 22 |
| 2.11 a) Current-time graph. b) The current-voltage graphs at different scan rate. | 26 |
| 2.12 Cyclic voltammogram result of a) 0.1 M Zn(NO ₃) ₂ , b) 0.5 mM eosin and c) 0.1 M Zn(NO ₃) ₂ + 0.5 mM eosin (Yoshida, <i>et al.</i> , 2000). | 26 |
| 2.13 Electron transfer reaction. | 27 |

| | | |
|------|--|----|
| 2.14 | a) The effect of the three different applied voltages on the Fermi-level in a metal. b) The reduction of a species in solution. | 28 |
| 3.1 | The face-centred cubic Bravais lattice (Kittel, 2005). | 30 |
| 3.2 | The structures of II-VI semiconductors a) zinc-blend and b) wurtzite (Esteves and Trindade, 2002). | 31 |
| 3.3 | Schematic picture of ionic core component of a three dimensional array of spherical symmetric potential of the crystal (Harrison, 2005). | 32 |
| 3.4 | The energy of electron states as a function of the wavevector k (Burkard, 2008). | 33 |
| 3.5 | Energy band scheme of a) direct band gap semiconductor $E_g = E_{\text{photon}}$ and b) indirect band gap semiconductor $E_g = E_{\text{photon}} + E_{\text{phonon}}$ | 34 |
| 3.6 | The relationship between the density of states and different system dimensions. | 36 |
| 3.7 | The discrete energy level of sub-bands in a) bulk and b) quantum structures. | 37 |
| 3.8 | The position of d -like levels of transition metal impurities related to valance band edges, the shaded bars, and the conduction band edges, white bars, in II-VI compounds (Tiablikov, 2013). | 40 |
| 3.9 | The splitting of states before and after the applied magnetic field. | 41 |
| 3.10 | The basic building block of α -Mn, the hexatetrahedron, is shown as a closed pack of twelve balls on the left and as stick model on the right (Farrow, <i>et al.</i> , 2013). | 42 |
| 3.11 | Infinite quantum well and its wave functions (Oppo, <i>et al.</i> , 1997). | 43 |
| 3.12 | Behaviour of infinite, finite quantum wells and superlattice (Oppo, <i>et al.</i> , 1997) | 44 |
| 3.13 | Optical absorption in bulk semiconductor and quantum wells, neglecting the excitonic effects (Oppo, <i>et al.</i> , 1997). | 45 |
| 3.14 | The one dimensional infinite well (Penc, <i>et al.</i> , 1996). | 47 |
| 3.15 | In-plane ($k_{x,y}$) dispersion curves and the subband structure (Bimberg, <i>et al.</i> , 1999). | 47 |
| 3.16 | The one dimensional finite well (Penc, <i>et al.</i> , 1996). | 48 |
| 3.17 | Electron effective mass m_e at the conduction band plotted versus light hole mass m_{lh} for some cubic group-IV, III-V and II-VI semiconductors. | |

| | | |
|------|---|----|
| | The solid line provides an approximate relation of $m_e = m_{lh}$ (Sadao, 2005). | 49 |
| 3.18 | A heterojunction formed with different bandgaps joined at two different semiconductor materials (Bimberg, <i>et al.</i> , 1999). | 50 |
| 3.19 | The one dimensional potential in the conduction and valance band occur at a heterojunction with two different materials (Harrison, 2005). | 50 |
| 3.20 | One dimensional potential in the conduction and valance bands for a single quantum well (left) and a stepped quantum well (right) (Harrison, 2005). | 51 |
| 3.21 | The one dimensional potential V in the conduction and valance band for: a) symmetric (left) and asymmetric (right) double quantum well, b) multiple quantum well or supperlattice (Harrison, 2005). | 51 |
| 3.22 | The one dimensional potential V in the conduction and valance band for type-I (left) and type-II (right) single quantum well system (Harrison, 2005). | 52 |
| 4.1 | Thin film experiment flowchart. | 54 |
| 4.2 | Heterostructure experiment flowchart. | 55 |
| 4.3 | Nanowire experiment flowchart. | 56 |
| 4.4 | ITO glass substrate. | 57 |
| 4.5 | The schematic diagram of electrodeposition set up. WE: working electrode, CE: counter electrode, RF: reference electrode. | 58 |
| 4.6 | Electrodeposition cell set up. | 59 |
| 4.7 | The schematic diagram of the heterostructure deposition from the top and side view. The electrolytes for the first and third solution were DMSs and the electrolyte of the second solution was ZnSe or ZnS. | 63 |
| 4.8 | Sputter coater. | 65 |
| 4.9 | Polycarbonate membrane with pore diameter of 200nm, a) before gold coating, b) after gold coating, c) ZnSe deposited, d) ZnS deposited. | 66 |
| 4.10 | As purchased polycarbonate membranes with pore diameter of a) 10nm, b) 100nm, c) 200nm and d) schematic picture of the PCTE after gold coating. | 66 |
| 4.11 | Potentiostat galvanostat AutoLab PGSTAT101 model. | 67 |

| | | |
|------|---|----|
| 4.12 | The circuit of potentiostat in a three-electrode cell and equipotential lines between reference and working electrode. | 67 |
| 4.13 | Schematic of the potentiostatic control loop. The control voltage forces a current through the counter electrode to achieve the wanted potential difference between WE and RE. | 68 |
| 4.14 | Scheme of x-ray diffraction applied in thin film measurement (Klockenkämper and von Bohlen, 2014). | 69 |
| 4.15 | Scattering of x-rays by a crystalline of simple cubic structure. X-ray is incident on a specimen and is diffracted by crystalline phase in specimen according to Bragg's law (Kittel, 2005). | 70 |
| 4.16 | Signals generated when a high energy beam of electrons interacts with a thin specimen. | 71 |
| 4.17 | Interaction volume and signals produce by interaction of electron beam and sample. | 72 |
| 4.18 | Schematic of AFM. | 73 |
| 4.19 | Sample holder of the UV-Visible spectroscopy. | 76 |
| 4.20 | a) different paths for radiative electron-hole recombination i) band to band, ii) donor to valance band, iii) conduction band to acceptor and b) non-radiative recombination via ab intermediate state (Kumaresan, <i>et al.</i> , 2002). | 77 |
| 4.21 | Diagram of the digital multimeter using constant current. | 78 |
| 4.22 | Schematic graph of two-point resistance measurement. | 78 |
| 4.23 | Schematic graph of four-point resistance measurement. | 79 |
| 4.24 | The photo of the two-point probe instrument. | 79 |
| 4.25 | Schematic diagram of the sample in VSM. | 80 |
| 4.26 | Diagram of the splitting of the energy levels. | 81 |
| 4.27 | ESR line shapes: a) Absorption spectrum, b) First derivative spectrum, c) Second derivative spectrum (Wertz, 2012). | 82 |
| 4.28 | The diagram of ESR spectrometer (Eaton, <i>et al.</i> , 1998). | 83 |
| 5.1 | Cyclic voltammogram for ITO electrode in 2 mL H ₂ SO ₄ and 100 mL deionized water, PH: 2.5-3. | 84 |

| | | |
|------|--|----|
| 5.2 | Cyclic voltammograms measured for three different Zn concentrations; a) 0.1 M ZnSO ₄ .7H ₂ O, b) 0.2 M ZnSO ₄ .7H ₂ O, c) 0.3 M ZnSO ₄ .7H ₂ O at room temperature and PH: 2.5-3.0. | 85 |
| 5.3 | Cyclic voltammograms measured for three different Se concentrations; a) 10 ⁻³ M SeO ₄ , b) 10 ⁻⁴ M SeO ₄ , c) 10 ⁻⁵ M SeO ₄ at room temperature and PH: 2.5-3.0. | 86 |
| 5.4 | Cyclic voltammograms measured for 10 ⁻³ M SeO ₄ at room temperature and PH: 2.5-3.0. | 87 |
| 5.5 | Cyclic voltammograms for deposition of ZnSe on ITO using 0.1 M ZnSO ₄ .7H ₂ O and a) 10 ⁻³ M SeO ₄ , b) 10 ⁻⁴ M SeO ₄ , c) 10 ⁻⁵ M SeO ₄ at room temperature and PH: 2.5-3.0. | 88 |
| 5.6 | Cyclic voltammograms for deposition of ZnSe on ITO using 0.2 M ZnSO ₄ .7H ₂ O and a) 10 ⁻³ M SeO ₄ , b) 10 ⁻⁴ M SeO ₄ , c) 10 ⁻⁵ M SeO ₄ at room temperature and PH: 2.5-3.0. | 89 |
| 5.7 | Cyclic voltammograms for deposition of ZnSe on ITO using 0.3 M ZnSO ₄ .7H ₂ O and a) 10 ⁻³ M SeO ₄ , b) 10 ⁻⁴ M SeO ₄ , c) 10 ⁻⁵ M SeO ₄ at room temperature and PH: 2.5-3.0. | 89 |
| 5.8 | Cyclic voltammograms for deposition of ZnSe-Mn on ITO using 0.1 M ZnSO ₄ .7H ₂ O + 10 ⁻³ M SeO ₄ solution and a) 1% , b) 5%, c) 10% MnSO ₄ .H ₂ O in respect to Zn ions at room temperature and PH: 2.5-3.0. | 90 |
| 5.9 | Chronoamperometric current-time graph of transient responses for ZnSe electrodeposition on ITO under deposition potential -0.5 V. | 91 |
| 5.10 | (I/I _m) ² vs. t/t _m analysis of transient response for ZnSe electrodeposition on ITO under deposition potential -0.65 V. Inset shows chronoamperometric current-time transients. | 92 |
| 5.11 | (I/I _m) ² vs. t/t _m analysis of transient response for ZnSe electrodeposition on ITO under deposition potential -0.8 V. Inset shows chronoamperometric current-time transients. | 92 |
| 5.12 | Current dependence vs time ^{-1/2} for ZnSe electrodeposition on ITO for a) -0.5 V, b) -0.65 V and c) -0.8 V deposition potential. | 93 |
| 5.13 | X-ray diffraction patterns of ZnSe films with different Zn to Se molar ratio deposited at -0.65 V for 30 minutes at 30°C. | 95 |
| 5.14 | X-ray diffraction patterns of ZnSe films with 0.1 M Zn and 10 ⁻³ M Se, deposited at different voltages for 30 minutes at 30 °C. | 96 |
| 5.15 | X-ray diffraction patterns of ZnSe films with 0.1 M Zn and 10 ⁻³ M Se, deposited at -0.95 V for 30 minutes at 30, 50, 70 and 90 °C. | 97 |

| | | |
|------|--|-----|
| 5.16 | X-ray diffraction patterns of ZnSe-Mn 1% films with 0.1 M Zn and 10^{-3} M Se, deposited at -0.95 V for 30 minutes at 30, 50, 70 and 90 °C. | 98 |
| 5.17 | X-ray diffraction patterns of ZnSe-Mn 5% films with 0.1 M Zn and 10^{-3} M Se, deposited at -0.95 V for 30 minutes at 30, 50, 70 and 90 °C. | 99 |
| 5.18 | X-ray diffraction patterns of ZnSe-Mn 10% films with 0.1 M Zn and 10^{-3} M Se, deposited at -0.95 V for 30 minutes at 30, 50, 70 and 90 °C. | 100 |
| 5.19 | Comparison between the peak intensity of ZnSe-Mn 1%, ZnSe-Mn 5 % and ZnSe-Mn 10% thin films deposited at four different deposition bath temperatures. | 101 |
| 5.20 | Enlarged (211) diffraction peaks of ZnSe doped with 1%, 5% and 10% Mn at 50 °C and 70 °C. | 101 |
| 5.21 | a) Dislocation density and b) strain versus Mn concentration for the samples deposited at different bath temperatures. ZnSe = 0%, ZnSe-Mn 1% = 1%, ZnSe-Mn 5% = 5% and ZnSe-Mn 10% = 10%. | 102 |
| 5.22 | FESEM micrographs of ZnSe films with 0.1 M Zn and 10^{-3} M Se, deposited at different voltages for 30 minutes at 30°C and their size distribution analysis. | 105 |
| 5.23 | FESEM micrographs of ZnSe films with 0.1 M Zn and 10^{-3} M Se, deposited at -0.65 V for 30 minutes at 30, 50, 70 and 90 °C in low magnification (left) and high magnification (right). | 106 |
| 5.24 | FESEM micrographs of ZnSe films with 0.1 M Zn and 10^{-3} M Se, deposited at -0.65 V for 5, 15, 30, 45, 60, 120, 180 minutes at 30°C in low magnification (left) and high magnification (right). | 109 |
| 5.25 | Cross section 45° FESEM image of ZnSe films on ITO glass substrate at deposition time a) 5 min, b) 15 min, c) 30 min, d) 45 min, e) 60 min, f) 120 min, g) 180 min and h) film thickness as a function of deposition time. | 110 |
| 5.26 | a) FESEM micrographs and b) EDX pattern of ZnSe films with 0.1 M Zn and 10^{-3} M Se, deposited at -0.65 V for 30 minutes at 30 °C. | 111 |
| 5.27 | a) FESEM micrographs and b) EDX pattern of ZnSe films with 0.1 M Zn and 10^{-3} M Se, deposited at -0.65 V for 30 minutes at 70 °C. | 112 |
| 5.28 | a) FESEM micrographs and b) EDX pattern of ZnSe films with 0.1 M Zn and 10^{-3} M Se, deposited at -0.65 V for 30 minutes at 30 °C. | 112 |
| 5.29 | a) FESEM micrographs and b) EDX pattern of ZnSe films with 0.1 M Zn and 10^{-3} M Se, deposited at -0.65 V for 180 minutes at 30 °C. | 112 |

| | | |
|------|--|-----|
| 5.30 | a) FESEM micrographs, b and c) EDX pattern of ZnSe films with 0.1 M Zn and 10^{-3} M Se, deposited at -0.65 V for 45 minutes at 30 °C. | 113 |
| 5.31 | FESEM micrographs of 1% Mn doped ZnSe films with 0.1 M Zn and 10^{-3} M Se, deposited at -0.95 V for 30 minutes at 30, 50, 70 and 90°C in low magnification (left) and high magnification (right). | 115 |
| 5.32 | The growth direction of ZnSe-Mn 1% thin film deposited at 70 °C in high magnification. | 115 |
| 5.33 | a) FESEM micrographs, b, c and d) EDX pattern of 1% Mn doped ZnSe films with 0.1 M Zn and 10^{-3} M Se, deposited at -0.95 V for 30 minutes at 90 °C. | 116 |
| 5.34 | FESEM micrographs of 5% Mn doped ZnSe films with 0.1 M Zn and 10^{-3} M Se, deposited at -0.95 V for 30 minutes at 30, 50, 70 and 90°C in low magnification (left) and high magnification (right). | 117 |
| 5.35 | a) FESEM micrographs, b and c) EDX pattern of 5% Mn doped ZnSe films with 0.1 M Zn and 10^{-3} M Se, deposited at -0.95 V for 30 minutes at 90 °C. | 118 |
| 5.36 | FESEM micrographs of 10% Mn doped ZnSe films with 0.1 M Zn and 10^{-3} M Se, deposited at -0.95 V for 30 minutes at 30, 50, 70 and 90 °C in low magnification (left) and high magnification (right). | 119 |
| 5.37 | a) FESEM micrographs, b, c and d) EDX pattern of 10% Mn doped ZnSe films with 0.1 M Zn and 10^{-3} M Se, deposited at -0.95 V for 30 minutes at 90 °C. | 120 |
| 5.38 | 3D and 2D AFM micrograph and surface cross section of the ZnSe thin film deposited for 5 minutes on ITO substrate. | 121 |
| 5.39 | 3D and 2D AFM micrograph and surface cross section of the ZnSe thin film deposited for 45 minutes on ITO substrate. | 122 |
| 5.40 | 3D and 2D AFM micrograph and surface cross section of the ZnSe thin film deposited for 120 minutes on ITO substrate. | 122 |
| 5.41 | 3D AFM micrograph of a) ZnSe-Mn 1%, b) ZnSe-Mn 5%, c) ZnSe-Mn 10% thin films deposited at 30 °C (left) and 70 °C (right) on ITO substrate. | 123 |
| 5.42 | Absorption spectra of ZnSe films deposited at different deposition voltages for 30 minutes at 30 °C. | 125 |
| 5.43 | Transmittance and reflectance spectra of ZnSe film deposited at -0.6 V for 30 minutes at 30 °C. | 125 |

| | | |
|------|--|-----|
| 5.44 | Transmittance spectra of ZnSe films deposited at different deposition voltages for 30 minutes at 30 °C. | 126 |
| 5.45 | Plot of $(\alpha h\nu)^2$ versus $h\nu$ for ZnSe thin films deposited at different deposition voltages for 30 minutes at 30°C. | 126 |
| 5.46 | Absorption spectra of ZnSe films deposited at different deposition bath temperatures for 30 minutes at -0.65 V. | 127 |
| 5.47 | Transmittance spectra of ZnSe films deposited at different deposition bath temperatures for 30 minutes at -0.65 V. | 127 |
| 5.48 | Plot of $(\alpha h\nu)^2$ versus $h\nu$ for ZnSe thin films deposited at different deposition bath temperatures for 30 minutes at -0.65 V. | 128 |
| 5.49 | Absorbance spectra of ZnSe thin films deposited at -0.65 V and 30 °C at different deposition time. | 129 |
| 5.50 | Transmittance spectra of ZnSe thin films deposited at -0.65 V and 30 °C at different deposition time. | 130 |
| 5.51 | Plot of $(\alpha h\nu)^2$ versus $h\nu$ for ZnSe thin films deposited at -0.65 V and 30 °C at different deposition time. | 130 |
| 5.52 | The energy bandgap as a function of deposition time. | 130 |
| 5.53 | Absorption spectra of: a) ZnSe-Mn 1%, b) ZnSe-Mn 5% and c) ZnSe-Mn 10% thin films deposited at different deposition bath temperatures for 30 minutes at -0.95 V. | 131 |
| 5.54 | Transmittance spectra of: a) ZnSe-Mn 1%, b) ZnSe-Mn 5% and c) ZnSe-Mn 10% thin films deposited at different deposition bath temperatures for 30 minutes at -0.95 V. | 132 |
| 5.55 | Plot of $(\alpha h\nu)^2$ versus $h\nu$ for: a) ZnSe-Mn 1%, b) ZnSe-Mn 5% and c) ZnSe-Mn 10% thin films deposited at different deposition bath temperatures for 30 minutes at -0.95 V. | 133 |
| 5.56 | Average grain size versus the bandgap energy for ZnSe-Mn 1%, 5% and 10%. | 134 |
| 5.57 | The relationship between the bandgap and manganese concentration for ZnSe-Mn thin films deposited at different deposition temperatures. The insert is the linear fitting graph. | 134 |
| 5.58 | PL spectra of ZnSe thin films deposited at different deposition voltages for 30 minutes at 30 °C. | 135 |
| 5.59 | PL spectra of ZnSe films deposited at different deposition bath temperatures for 30 minutes at -0.65 V. | 136 |

| | | |
|------|--|-----|
| 5.60 | PL spectra of ZnSe thin films deposited at -0.65 V and 30 °C at different deposition time. | 137 |
| 5.61 | PL spectra of ZnSe-Mn 1% films deposited at different deposition bath temperatures for 30 minutes at -0.95 V. | 138 |
| 5.62 | PL spectra of ZnSe-Mn 5% films deposited at different deposition bath temperatures for 30 minutes at -0.95 V. | 138 |
| 5.63 | PL spectra of ZnSe-Mn 10% films deposited at different deposition bath temperatures for 30 minutes at -0.95 V. | 139 |
| 5.64 | A Compare between the PL spectra of 1%, 5% and 10% Mn-doped ZnSe thin films. | 140 |
| 5.65 | Energy level diagram for the Mn-doped ZnSe quantum structures. (VB: valence band, CB: conduction band, ST: surface traps). | 140 |
| 5.66 | Current-voltage characteristic curve for ZnSe thin films deposited at -1.0 V in bath temperature of 30 °C for 30 minutes. | 141 |
| 5.67 | Current-voltage characteristic curves for ZnSe thin films deposited at -0.65 V in different bath temperatures for 30 minutes. | 141 |
| 5.68 | The relationship between the resistivity and film thickness and average grain size. | 142 |
| 5.69 | Current-voltage characteristic curves for ZnSe thin films deposited at -0.65 V and 30 °C at different deposition time. | 143 |
| 5.70 | The electron scattering at the grain boundaries and path of electron that scattered from grain boundary to grain boundary. Mean path is equal to grain size. | 143 |
| 5.71 | Current-voltage characteristic curves for ZnSe-Mn 1%, 5% and 10% thin films deposited at bath temperature 70 °C for 30 minutes and -0.95 V. | 144 |
| 5.72 | Magnetic moment as a function of applied magnetic field of 1% Mn-doped ZnSe thin film deposited at: a) 70 °C and b) 90 °C. | 145 |
| 5.73 | Magnetic moment as a function of applied magnetic field of 5% Mn-doped ZnSe thin film deposited at: a) 70 °C and b) 90 °C. | 146 |
| 5.74 | Magnetic moment as a function of applied magnetic field of 10% Mn-doped ZnSe thin film deposited at: a) 70 °C and b) 90 °C. | 147 |
| 5.75 | ESR spectrum of sample holder without sample. | 148 |

| | | |
|------|---|-----|
| 5.76 | Electron Zeeman splitting as a function of the magnetic field and the resonance condition. | 149 |
| 5.77 | ESR spectra of ZnSe thin films doped with 1%, 5% and 10% manganese concentration deposited at 70 °C. | 151 |
| 5.78 | Cyclic voltammograms for deposition of ZnS on ITO using a) 0.01 M ZnSO ₄ .7H ₂ O + 0.01 M Na ₂ S ₂ O ₃ .5H ₂ O and b) 0.025 M ZnSO ₄ .7H ₂ O + 0.01 M Na ₂ S ₂ O ₃ .5H ₂ O at room temperature and PH: 3.5-4.0. | 152 |
| 5.79 | Cyclic voltammograms for deposition of ZnS on ITO using a) 0.01 M ZnSO ₄ .7H ₂ O + 0.01 M C ₂ H ₅ NS and b) 0.01 M ZnSO ₄ .7H ₂ O + 0.01 M Na ₂ S.H ₂ O at room temperature and PH: 3.5-4.0. | 152 |
| 5.80 | Cyclic voltammograms for deposition of ZnS-Mn on ITO using 0.025 M ZnSO ₄ .7H ₂ O + 0.01 M Na ₂ S ₂ O ₃ .5H ₂ O and; a) 1% , b) 5%, c) 10% MnSO ₄ .H ₂ O in respect to Zn ions at room temperature and PH: 3.5-4.0. | 153 |
| 5.81 | (I/I _m) ² vs. t/t _m analysis of transient response for ZnS electrodeposition on ITO under deposition potential -0.9 V. Inset shows chronoamperometric current-time transients. | 154 |
| 5.82 | (I/I _m) ² vs. t/t _m analysis of transient response for ZnS electrodeposition on ITO under deposition potential -1.1 V. Inset shows chronoamperometric current-time transients. | 155 |
| 5.83 | (I/I _m) ² vs. t/t _m analysis of transient response for ZnS electrodeposition on ITO under deposition potential -1.3 V. Inset shows chronoamperometric current-time transients. | 155 |
| 5.84 | Current dependence vs time ^{-1/2} for ZnS electrodeposition on ITO for a) -0.9 V, b) -1.1 V and c) -1.3 V deposition potential. | 156 |
| 5.85 | X-ray diffraction patterns of ZnS films deposited at -1.1 V for 30 minutes at 70 °C. S1: 0.01 M ZnSO ₄ .7H ₂ O + 0.05 M Na ₂ S ₂ O ₃ .5H ₂ O, S2: 0.025 M ZnSO ₄ .7H ₂ O + 0.01 M Na ₂ S ₂ O ₃ .5H ₂ O, S3: 0.01 M ZnSO ₄ .7H ₂ O + 0.01 M C ₂ H ₅ NS, S4: 0.01 M ZnSO ₄ .7H ₂ O + 0.01 M Na ₂ S.H ₂ O. | 157 |
| 5.86 | X-ray diffraction patterns of ZnS films with 0.025 M ZnSO ₄ .7H ₂ O and 0.01 M Na ₂ S ₂ O ₃ .5H ₂ O, deposited at different voltages for 30 minutes at 30 °C. | 159 |
| 5.87 | X-ray diffraction patterns of ZnS films with 0.025 M ZnSO ₄ .7H ₂ O and 0.01 M Na ₂ S ₂ O ₃ .5H ₂ O, deposited at -1.1 V for 30 minutes at 30, 50, 70 and 90 °C. | 160 |
| 5.88 | X-ray diffraction patterns of ZnS-Mn 1% films with 0.025 M ZnSO ₄ .7H ₂ O and 0.01 M Na ₂ S ₂ O ₃ .5H ₂ O, deposited at -1.25 V for 30 minutes at 30, 50, 70 and 90 °C. | 161 |

| | | |
|-------|--|-----|
| 5.89 | Comparison between the XRD patter of ZnS-Mn 1% and the reference pattern. Pie chart shows the contribution percentage of $Zn_{0.98}Mn_{0.02}S$, cubic ZnS, hexagonal ZnS and Zn. | 162 |
| 5.90 | X-ray diffraction patterns of ZnS-Mn 5% films with 0.025 M $ZnSO_4 \cdot 7H_2O$ and 0.01 M $Na_2S_2O_3 \cdot 5H_2O$, deposited at -1.25 V for 30 minutes at 30, 50, 70 and 90 °C. | 163 |
| 5.91 | Comparison between the XRD patter of ZnS-Mn 5% and the reference pattern. Pie chart shows the contribution percentage of $Zn_{0.48}Mn_{0.52}S$, cubic ZnS, hexagonal ZnS and Zn. | 163 |
| 5.92 | X-ray diffraction patterns of ZnS-Mn 10% films with 0.025 M $ZnSO_4 \cdot 7H_2O$ and 0.01 M $Na_2S_2O_3 \cdot 5H_2O$, deposited at -1.25 V for 30 minutes at 30, 50, 70 and 90 °C. | 165 |
| 5.93 | Comparison between the XRD patter of ZnS-Mn 10% and the reference pattern. Pie chart shows the contribution percentage of $Zn_{0.73}Mn_{0.27}S$, cubic ZnS, hexagonal ZnS and Zn. | 165 |
| 5.94 | Comparison between the peak intensity of ZnS-Mn 1%, ZnS-Mn 5% and ZnS-Mn 10% thin films deposited at four different deposition bath temperatures. | 166 |
| 5.95 | Enlarged (110) diffraction peaks of ZnS doped with 1%, 5% and 10% Mn at 30 °C, 50 °C, 70 °C and 90 °C. | 166 |
| 5.96 | Manganese percentage concentration versus lattice parameters of ZnS-Mn thin films. | 167 |
| 5.97 | Dislocation density and strain versus Mn concentration for the samples deposited at different bath temperatures. ZnS = 0%, ZnS-Mn 1% = 1%, ZnS-Mn 5% = 5% and ZnS-Mn 10% = 10%. | 168 |
| 5.98 | FESEM micrograph and EDX pattern of ZnS film for sample S2 (0.025 M $ZnSO_4 \cdot 7H_2O$ + 0.01 M $Na_2S_2O_3 \cdot 5H_2O$) deposited at -1.1 V for 30 minutes at 30 °C. | 169 |
| 5.99 | FESEM micrographs of ZnS films deposited at -1.1 V for 30 minutes at 70 °C. S1: 0.01 M $ZnSO_4 \cdot 7H_2O$ + 0.05 M $Na_2S_2O_3 \cdot 5H_2O$, S2: 0.025 M $ZnSO_4 \cdot 7H_2O$ + 0.01 M $Na_2S_2O_3 \cdot 5H_2O$, S3: 0.01 M $ZnSO_4 \cdot 7H_2O$ + 0.01 M C_2H_5NS , S4: 0.01 M $ZnSO_4 \cdot 7H_2O$ + 0.01 M $Na_2S \cdot H_2O$. | 169 |
| 5.100 | FESEM micrographs of ZnS films with 0.025 M $ZnSO_4 \cdot 7H_2O$ and 0.01 M $Na_2S_2O_3 \cdot 5H_2O$, deposited at different voltages for 30 minutes at 30 °C and their size distribution analysis. | 171 |
| 5.101 | FESEM micrographs and EDX patterns of ZnS film deposited at a) -0.9 V, b) -1.1 V and c) -1.3 V for 30 minutes at 30 °C. | 172 |

| | | |
|-------|---|-----|
| 5.102 | FESEM micrographs of ZnS films with 0.025 M ZnSO ₄ .7H ₂ O and 0.01 M Na ₂ S ₂ O ₃ .5H ₂ O, deposited at -1.1 V for 30 minutes at 30, 50, 70 and 90 °C. | 174 |
| 5.103 | Cross section 45° FESEM image of ZnS films on ITO glass substrate at different deposition temperatures. | 174 |
| 5.104 | FESEM micrographs and EDX patterns of ZnS film deposited at -1.1 V for 30 minutes at a) 70 °C and b) 90 °C. | 175 |
| 5.105 | FESEM micrographs of ZnS films with 0.025 M ZnSO ₄ .7H ₂ O and 0.01M Na ₂ S ₂ O ₃ .5H ₂ O, deposited at -1.1 V for 5, 15, 30, 45, 60, 120, 180 minutes at 30 °C in low magnification (left) and high magnification (right). | 177 |
| 5.106 | The enlarge image of the cluster formed in sample deposited for 180 minutes. | 178 |
| 5.107 | Cross section 45° FESEM image of ZnS films on ITO glass substrate at deposition time a) 5 min, b) 15 min, c) 30 min, d) 45 min, e) 60 min, f) 120 min, g) 180 min and h) film thickness as a function of deposition time. | 179 |
| 5.108 | FESEM micrographs of ZnS-Mn 1% films with 0.025 M ZnSO ₄ .7H ₂ O and 0.01 M Na ₂ S ₂ O ₃ .5H ₂ O, deposited at -1.25 V for 30 minutes at 30, 50, 70 and 90 °C. | 180 |
| 5.109 | FESEM micrographs of ZnS-Mn 5% films with 0.025 M ZnSO ₄ .7H ₂ O and 0.01 M Na ₂ S ₂ O ₃ .5H ₂ O, deposited at -1.25 V for 30 minutes at 30, 50, 70 and 90 °C. | 181 |
| 5.110 | FESEM micrographs of ZnS-Mn 10% films with 0.025 M ZnSO ₄ .7H ₂ O and 0.01 M Na ₂ S ₂ O ₃ .5H ₂ O, deposited at -1.25 V for 30 minutes at 30, 50, 70 and 90 °C. | 182 |
| 5.111 | FESEM micrographs, and EDX patterns of ZnS-Mn films a) 1%, b) 5% and c) 10% deposited at 70 °C. | 183 |
| 5.112 | 3D and 2D AFM micrograph and surface cross section of the ZnS thin film deposited for 30 minutes on ITO substrate. | 184 |
| 5.113 | 3D and 2D AFM micrograph and surface cross section of the ZnS thin film deposited for 60 minutes on ITO substrate. | 184 |
| 5.114 | 3D AFM micrograph of a) ZnS-Mn 1%, b) ZnS-Mn 5%, c) ZnS-Mn 10% thin films deposited at 30 °C (left) and 70 °C (right) on ITO substrate. | 185 |
| 5.115 | Absorption spectra of ZnS films deposited at different deposition voltages for 30 minutes at 30 °C. | 186 |

| | | |
|-------|--|-----|
| 5.116 | Transmittance spectra of ZnS films deposited at different deposition voltages for 30 minutes at 30 °C. | 187 |
| 5.117 | Plot of $(\alpha hv)^2$ versus hv for ZnS thin films deposited at different deposition voltages for 30 minutes at 30 °C. | 187 |
| 5.118 | Absorption spectra of ZnS films deposited at different deposition bath temperatures for 30 minutes at -1.1 V. | 188 |
| 5.119 | Transmittance spectra of ZnS films deposited at different deposition bath temperatures for 30 minutes at -1.1 V. | 189 |
| 5.120 | Plot of $(\alpha hv)^2$ versus hv for ZnS thin films deposited at different deposition bath temperatures for 30 minutes at -1.1 V. | 189 |
| 5.121 | Absorption spectra of ZnS thin films deposited at -1.1 V and 70 °C at different deposition time. | 190 |
| 5.122 | Transmittance spectra of ZnS thin films deposited at -1.1 V and 70 °C at different deposition time. | 190 |
| 5.123 | Plot of $(\alpha hv)^2$ versus hv for ZnS thin films deposited at -1.1 V and 70 °C at different deposition time. | 191 |
| 5.124 | Absorption spectra of: a) ZnS-Mn 1%, b) ZnS-Mn 5% and c) ZnS-Mn 10% thin films deposited at different deposition bath temperatures for 30 minutes at -1.25 V. | 192 |
| 5.125 | Transmittance spectra of: a) ZnS-Mn 1%, b) ZnS-Mn 5% and c) ZnS-Mn 10% thin films deposited at different deposition bath temperatures for 30 minutes at -1.25 V. | 193 |
| 5.126 | Plot of $(\alpha hv)^2$ versus hv for: a) ZnS-Mn 1%, b) ZnS-Mn 5% and c) ZnS-Mn 10% thin films deposited at different deposition bath temperatures for 30 minutes at -1.25 V. Left is the graph of temperature versus bandgap energy and the grain size. | 194 |
| 5.127 | The relationship between the bandgap and manganese concentration for ZnS-Mn thin films deposited at different deposition temperatures. | 195 |
| 5.128 | PL spectra of ZnS thin films deposited at different deposition voltages for 30 minutes at 30 °C. | 196 |
| 5.129 | PL spectra of ZnS films deposited at different deposition bath temperatures for 30 minutes at -1.1 V. | 197 |
| 5.130 | PL spectra of ZnS thin films deposited at -1.1 V and 30 °C at different deposition time. | 197 |
| 5.131 | Photo-generated electron-hole in ZnS thin film. | 198 |

| | | |
|-------|--|-----|
| 5.132 | PL spectra of ZnS-Mn 1% thin films deposited at different deposition bath temperatures for 30 minutes at -1.25 V. | 199 |
| 5.133 | PL spectra of ZnS-Mn 5% thin films deposited at different deposition bath temperatures for 30 minutes at -1.25 V. | 199 |
| 5.134 | PL spectra of ZnS-Mn 10% thin films deposited at different deposition bath temperatures for 30 minutes at -1.25 V. | 200 |
| 5.135 | PL spectra of un-doped (Mn 0%) and Mn-doped (1%, 5%, 10%) ZnS thin films deposited at 70 °C. | 201 |
| 5.136 | Current-voltage characteristic curves for ZnS thin films deposited at -1.1 V in different bath temperatures for 30 minutes. | 202 |
| 5.137 | Current-voltage characteristic curves for ZnS thin films deposited at -1.1 V and 70 °C for 5, 15, 45 and 60 minutes. | 202 |
| 5.138 | Current-voltage characteristic curves for ZnS-Mn 1%, 5% and 10% thin films deposited at bath temperature 70 °C for 30 minutes and -1.25 V. $R \Omega$, $\rho \Omega nm$, $\sigma (1 \Omega nm)$ versus Mn concentration. | 203 |
| 5.139 | Magnetic moment as a function of applied magnetic field of 1% Mn-doped ZnS thin film deposited at: a) 70 °C and b) 90 °C. | 204 |
| 5.140 | Magnetic moment as a function of applied magnetic field of 5% Mn-doped ZnS thin film deposited at: a) 70 °C and b) 90 °C. | 205 |
| 5.141 | Magnetic moment as a function of applied magnetic field of 10% Mn-doped ZnS thin film deposited at: a) 70 °C and b) 90 °C. | 206 |
| 5.142 | ESR spectra of ZnS thin film doped with 1%, 5% and 10% manganese concentration deposited at 70 °C. | 208 |
| 5.143 | X-ray diffraction patterns of heterostructure $Zn_{0.985}Mn_{0.015}Se/ZnSe/Zn_{0.985}Mn_{0.015}Se$ with three different ZnSe quantum well thickness. | 210 |
| 5.144 | The graph of FWHM and crystallite size of quantum well ZnSe versus the deposition time. Pie chart shows the percentage of ZnSe and $Zn_{0.985}Mn_{0.015}Se$ in XRD peaks. | 210 |
| 5.145 | FESEM micrographs of ZnMnSe/ZnSe/ZnMnSe 1% with different quantum well thickness (t_{ZnSe}) deposited for: a) 5 min, b) 15 min and c) 30 min in low (left) and high (right) magnification. | 212 |
| 5.146 | FESEM micrograph and EDX spectrums of ZnMnSe/ZnSe/ZnMnSe 1%. | 213 |

| | | |
|-------|--|-----|
| 5.147 | FESEM micrographs of ZnMnSe/ZnSe/ZnMnSe 5% with different quantum well thickness (t_{ZnSe}) deposited for: a) 5 min, b) 15 min and c) 30 min in low (left) and high (right) magnification. | 214 |
| 5.148 | FESEM micrographs of ZnMnSe/ZnSe/ZnMnSe 10% with different quantum well thickness (t_{ZnSe}) deposited for: a) 5 min, b) 15 min and c) 30 min in low (left) and high (right) magnification. | 215 |
| 5.149 | Cross section 45° FESEM image of ZnMnSe/ZnSe/ZnMnSe 1% heterostructure on ITO glass substrate with different quantum well thickness (t_{ZnSe}) deposited for: a) 5 min, b) 15 min and c) 30 min. | 216 |
| 5.150 | Cross section 45° FESEM image of ZnMnSe/ZnSe/ZnMnSe 10% heterostructure on ITO glass substrate with different quantum well thickness (t_{ZnSe}) deposited for: a) 5 min, b) 15 min and c) 30 min. | 217 |
| 5.151 | Thickness measurement result of ZnMnSe/ZnSe/ZnMnSe heterostructure with ZnSe quantum well deposited for 5 minutes and Mn concentration of 5%. | 218 |
| 5.152 | Absorbance spectra of heterostructure ZnMnSe/ZnSe/ZnMnSe with three different ZnSe quantum well thickness, and Mn concentrations: a) 1%, b) 5% and c) 10%. | 220 |
| 5.153 | Transmittance spectra of heterostructure ZnMnSe/ZnSe/ZnMnSe with three different ZnSe quantum well thickness, and Mn concentrations: a) 1%, b) 5% and c) 10%. | 221 |
| 5.154 | Plot of $(\alpha h\nu)^2$ versus $h\nu$ for heterostructure ZnMnSe/ZnSe/ZnMnSe with three different ZnSe quantum well thickness and Mn concentrations: a) 1%, b) 5% and c) 10%. | 222 |
| 5.155 | PL spectra of heterostructure ZnMnSe/ZnSe/ZnMnSe a) 1%, b) 5% and c) 10% with three different ZnSe quantum well thickness as function of wavelength and energy. | 224 |
| 5.156 | PL spectra of (Zn,Mn)Se/ZnSe heterostructures as a function of a) wavelength and b) photon energy (eV). | 225 |
| 5.157 | The FWHM of the photoluminescence emission peak versus the ZnSe quantum well deposition time. | 226 |
| 5.158 | The schematic diagram of single quantum well ZnSe heterostructure and band structure of ZnSe single quantum well. | 226 |
| 5.159 | Current-voltage characteristics of ZnMnSe/ZnSe/ZnMnSe heterostructure with 1% Mn concentration and different ZnSe well thickness. | 228 |
| 5.160 | Current-voltage characteristics of ZnMnSe/ZnSe/ZnMnSe heterostructure with 5% Mn concentration and different ZnSe well thickness. | 229 |

| | | |
|-------|--|-----|
| 5.161 | Current-voltage characteristics of ZnMnSe/ZnSe/ZnMnSe heterostructure with 10% Mn concentration and different ZnSe well thickness. | 230 |
| 5.162 | Current-voltage characteristics of heterostructure at the junction between a) ITO substrate and first layer ZnMnSe quantum barrier and b) ITO substrate and third layer ZnMnSe quantum barrier. | 231 |
| 5.163 | Current-voltage characteristics of heterostructure at the junction between ZnSe quantum well and ZnMnSe quantum barriers. | 232 |
| 5.164 | Current-voltage characteristics of heterostructure between two ZnMnSe quantum barriers. | 233 |
| 5.165 | ESR spectra of heterostructure ZnMnSe/ZnSe/ZnMnSe doped with 1%, 5% and 10% manganese concentration. | 235 |
| 5.166 | Schematic of the band profile of spin-up and spin-down electrons. | 236 |
| 5.167 | X-ray diffraction patterns of heterostructure $Zn_{0.99}Mn_{0.01}S/ZnS/Zn_{0.99}Mn_{0.01}S$ with three different ZnS quantum well thickness. | 237 |
| 5.168 | FESEM micrographs of ZnMnS/ZnS/ZnMnS 1% with different quantum well thickness (t_{ZnS}) deposited for: a) 5 min, b) 15 min and c) 30 min in low (left) and high (right) magnification. | 239 |
| 5.169 | FESEM micrographs of ZnMnS/ZnS/ZnMnS 5% with different quantum well thickness (t_{ZnS}) deposited for: a) 5 min, b) 15 min and c) 30 min in low (left) and high (right) magnification. | 240 |
| 5.170 | FESEM micrographs of ZnMnS/ZnS/ZnMnS 10% with different quantum well thickness (t_{ZnS}) deposited for: a) 5 min, b) 15 min and c) 30 min in low (left) and high (right) magnification. | 241 |
| 5.171 | FESEM micrographs and EDX spectrums of ZnMnS/ZnS/ZnMnS a) 1%, b) 5% and c) 10%. | 242 |
| 5.172 | Cross section 45° FESEM image of ZnMnS/ZnS/ZnMnS 1% heterostructure on ITO glass substrate with different quantum well thickness (t_{ZnSe}) deposited for: a) 5 min, b) 15 min and c) 30 min. | 244 |
| 5.173 | Cross section 45° FESEM image of ZnMnS/ZnS/ZnMnS 10% heterostructure on ITO glass substrate with different quantum well thickness (t_{ZnSe}) deposited for: a) 5 min, b) 15 min and c) 30 min. | 245 |
| 5.174 | Absorbance spectra of heterostructure ZnMnS/ZnS/ZnMnS with three different ZnS quantum well thickness, and Mn concentrations: a) 1%, b) 5% and c) 10%. | 247 |

| | | |
|-------|--|-----|
| 5.175 | Transmittance spectra of heterostructure ZnMnS/ZnS/ZnMnS with three different ZnS quantum well thickness, and Mn concentrations: a) 1%, b) 5% and c) 10%. | 248 |
| 5.176 | Plot of $(\alpha hv)^2$ versus hv for heterostructure ZnMnS/ZnS/ZnMnS with three different ZnS quantum well thickness, and Mn concentrations: a) 1%, b) 5% and c) 10%. | 249 |
| 5.177 | PL spectra of heterostructure ZnMnS/ZnS/ZnMnS a) 1%, b) 5% and c) 10% with three different ZnS quantum well thickness as function of wavelength and energy. | 251 |
| 5.178 | PL spectra of (Zn,Mn)S/ZnS heterostructures as a function of wavelength. | 252 |
| 5.179 | The FWHM of the photoluminescence emission peak versus the ZnS quantum well deposition time. | 252 |
| 5.180 | Models of the interface structure related to the size of the exciton wavefunction : a) two rough interfaces; b) one smooth and one rough interface; c) two smooth interfaces (Gfroerer, 2000). | 253 |
| 5.181 | Current-voltage characteristics of ZnMnS/ZnS/ZnMnS heterostructure with 1% Mn concentration and different ZnS well thickness. | 254 |
| 5.182 | Current-voltage characteristics of ZnMnS/ZnS/ZnMnS heterostructure with 5% Mn concentration and different ZnS well thickness. | 254 |
| 5.183 | Current-voltage characteristics of ZnMnS/ZnS/ZnMnS heterostructure with 10% Mn concentration and different ZnS well thickness. | 255 |
| 5.184 | Current-voltage characteristics of heterostructure at the junction between a) ITO substrate and first layer ZnMnS quantum barrier and b) ITO substrate and third layer ZnMnS quantum barrier. | 256 |
| 5.185 | Current-voltage characteristics of heterostructure at the junction between ZnS quantum well and ZnMnS quantum barriers. | 257 |
| 5.186 | Current-voltage characteristics of heterostructure between two ZnMnS quantum barriers. | 257 |
| 5.187 | ESR spectra of heterostructure ZnMnS/ZnS/ZnMnS doped with 1%, 5% and 10% manganese concentration. | 260 |
| 5.188 | FESEM images and EDX spectrums of the ZnSe nanowires grown in PCTE with pore diameter of a) 10, b) 100 and c) 200 nm. | 261 |
| 5.189 | FESEM images of the ZnSe-Mn nanowires grown in PCTE with pore diameter of a) 10, b) 200 and c) 100 nm. | 262 |

| | | |
|-------|---|-----|
| 5.190 | EDX spectrums of the ZnSe-Mn 10% nanowires grown in PC TE with 100 nm pore diameter. | 263 |
| 5.191 | TEM images of ZnSe nanowires in high (left) and low (right) magnification. | 264 |
| 5.192 | Absorbance spectra of ZnSe nanowires grown in PC TE with pore diameter 10 nm, 100 nm, 200 nm. | 265 |
| 5.193 | Transmittance and reflectance spectra of ZnSe nanowires grown in PC TE with pore diameter 10 nm, 100 nm, 200 nm. | 265 |
| 5.194 | Plot of $(ah\nu)^2$ versus $h\nu$ for ZnSe nanowires grown in PC TE with pore diameter 10 nm, 100 nm, 200 nm. | 266 |
| 5.195 | Absorbance and transmittance spectra of Mn-doped ZnSe nanowires grown in PC TE with pore diameter 10 nm, 100 nm, 200 nm and manganese concentration of: a) 1% Mn, b) 5% Mn and c) 10% Mn. | 267 |
| 5.196 | Plot of $(ah\nu)^2$ versus $h\nu$ for Mn-doped ZnSe nanowires grown in PC TE with pore diameter 10 nm, 100 nm, 200 nm and manganese concentration of: a) 1% Mn, b) 5% Mn and c) 10% Mn. | 269 |
| 5.197 | Current-voltage characteristic curves for ZnSe nanowires grown in PC TE with pore diameters of 10 nm, 100 nm, 200 nm. | 270 |
| 5.198 | Current-voltage characteristic curves for ZnSe-Mn 1% nanowires grown in PC TE with pore diameters of 10 nm, 100 nm, 200 nm. | 271 |
| 5.199 | Current-voltage characteristic curves for ZnSe-Mn 5% nanowires grown in PC TE with pore diameters of 10 nm, 100 nm, 200 nm. | 271 |
| 5.200 | Current-voltage characteristic curves for ZnSe-Mn 10% nanowires grown in PC TE with pore diameters of 10 nm, 100 nm, 200 nm. | 272 |
| 5.201 | FESEM images in low and high magnification and EDX spectrums of the ZnS nanowires grown in PC TE with pore diameter of 10 nm. | 273 |
| 5.202 | FESEM images in low and high magnification and EDX spectrums of the ZnS nanowires grown in PC TE with pore diameter of 100 nm. | 274 |
| 5.203 | FESEM images in low and high magnification and EDX spectrums of the ZnS nanowires grown in PC TE with pore diameter of 200 nm. | 275 |
| 5.204 | FESEM images of the ZnS-Mn nanowires grown in PC TE with pore diameter of a) 10, b) 200 and c) 100 nm. | 276 |
| 5.205 | FESEM images and EDX spectrums of the ZnS-Mn nanowires grown in PC TE with pore diameter of a) 10 nm, b) 200 nm and c) 100 nm. | 277 |

| | | |
|-------|---|-----|
| 5.206 | TEM images of ZnS nanowire in high magnification. | 277 |
| 5.207 | Absorbance spectra of ZnS nanowires grown in PCTE with pore diameter 10 nm, 100 nm, 200 nm. | 278 |
| 5.208 | Transmittance spectra of ZnS nanowires grown in PCTE with pore diameter 10 nm, 100 nm, 200 nm. | 278 |
| 5.209 | Plot of $(\alpha h\nu)^2$ versus $h\nu$ for ZnS nanowires grown in PCTE with pore diameter 10 nm, 100 nm, 200 nm. | 279 |
| 5.210 | Absorbance and transmittance spectra of Mn-doped ZnS nanowires grown in PCTE with pore diameter 10 nm, 100 nm, 200 nm and manganese concentration of: a) 1% Mn, b) 5% Mn and c) 10% Mn. | 280 |
| 5.211 | Plot of $(\alpha h\nu)^2$ versus $h\nu$ for Mn-doped ZnS nanowires grown in PCTE with pore diameter 10 nm, 100 nm, 200 nm and manganese concentration of: a) 1% Mn, b) 5% Mn and c) 10% Mn. | 282 |
| 5.212 | Current-voltage characteristic curves for ZnS nanowires grown in PCTE with pore diameters of 10 nm, 100 nm, 200 nm. | 283 |
| 5.213 | Current-voltage characteristic curves for ZnS-Mn 1% nanowires grown in PCTE with pore diameters of 10 nm, 100 nm, 200 nm. | 284 |
| 5.214 | Current-voltage characteristic curves for ZnS-Mn nanowires with different Mn concentration grown in PCTE with pore diameters of 200 nm. | 285 |

LIST OF ABBREVIATIONS

| | |
|----------------|--------------------------------------|
| Å | Angstroms |
| AAM | Anodic alumina membran |
| AFM | Antiferromagnet |
| BSE | Backscattered electrons |
| 1D | One-dimensional |
| 2D | Two-dimensional |
| CB | Conduction band |
| σ | Conductivity |
| D | Diameter |
| DMS | Dilute magnetic semiconductors |
| DL | Double layer |
| δ | Dislocation density |
| emu/g | Electromagnetic unit per gram |
| ESR | Electron spin resonance |
| ED | Electrodeposition |
| EDX | Energy dispersive x-ray spectroscopy |
| FWHM | Full width at half maximum |
| FM | Ferromagnet |
| g | Gram |
| GMR | Giant magneto resistance |
| H | Magnetic field strength |
| H _C | Coercivity |
| H _E | Exchange bias filed |
| nm | Nanometer |
| NPs | nanoparticles |
| M _r | Remanent magnetization |
| M _s | Saturation magnetization |
| MBE | Molecular beam epitaxy |
| MR | magnetoresistance |
| Oe | Orsted |
| PCTE | Polycarbonate |
| PL | Photoluminescence |
| ρ | Resistivity |
| QD | Quantum dot |
| QW | Quantum well, quantum wire |
| R | Resistance |
| UHV | Ultra-high vacuum |
| SE | Secondary electrons |
| V | Volume |
| X | Magnetic susceptibility |
| XRD | X-ray diffraction |

CHAPTER 1

INTRODUCTION

1.1 Background of the study

Low dimensional structures refer to systems in which at least one of the three dimensions is intermediate between the characteristic of atoms/molecules generally in the range of 1 to 100 nm. In low dimension electron systems, one or more spatial dimensions are small enough to restrict the quantum mechanical wave-function of electrons. The electrons contained inside, exhibit some diverse and interesting physical phenomena in all of the condensed matter physics. Two-dimensional structures, nanowires, nanotubes and quantum dots are examples of low dimensional systems. In these systems the surface states become important and even dominant due to high surface area to volume ratio. Additionally the dimensional restriction on the system gives rise to quantum size effects that significantly change their behaviour and energy spectrum of electrons. Consequently the properties of such systems are identically different from those of bulk counterparts and they show extraordinary electronic, optical, magnetic and chemical properties, which may result in their use in wide range of nanotechnology.

In recent years an extraordinary volume of research has been carried out on low dimensional semiconductors, metals, ceramics, and composites containing nanostructure materials for application in health/disease, sensing systems, electronics and communication, information processing and storage using multiple functional nanomaterials. Quantum structures have superior charge transport and optical properties thus much intensive research has been done to use them in making diode lasers, transistors and biological sensors. Improved technology for growing semiconductor thin film of different structural and electronic properties with layer thickness approaching atomic dimensions have provided new opportunities for basic scientific studies and device applications.

Advances in multilayer thin film growth techniques such as molecular beam epitaxy (Bimberg *et al.*, 1999) and metal organic chemical vapour deposition (MOCVD)(Warren, *et al.*, 2015) have made it possible to produce semiconductor heterojunctions between IV-IV, III-V, and II-VI compounds with tailored electronic and optical properties that do not occur in nature. The epitaxial layers using the advanced methods are so thin that quantum mechanical effects in the operation of heterostructure devices have been realized. It is also possible to control the alloy composition and doping in ternary and quaternary IV-IV, III-V, and II-VI semiconductor compounds over atomic distances.

1.2 Introduction to spintronics

For many years magnetism has been the basis for information process and storage. The field of spintronics was initiated with the discovery of the giant magneto-

resistive (GMR) effect in 1988 (Maekawa and Shinjo, 2002). In GMRs the resistance of the sandwiched thin film ferromagnetic and nonmagnetic multi-layers are strongly depend on magnetic field. Nowadays GMR effect is applied almost in every modern computer hard drive. Further advances in this area come from new type of magnetic devices which manipulate both spin and charge of the electron. These devices are called spintronics which lead to more exotic information devices and capable of wide variety of functionality.

The combination of magnetism (spin) and semiconductivity (charge) in one device to store and process the information is tomorrow's information technology. The technology utilizing the degrees of freedom in both charge and spin, called spintronics or spin electronics, is one of the hot topics today and has raised much research interest by implementing novel functionalities in the community of electronics and magnetics. The charge, mass and spin of electrons form the foundation of present information technology.

Most magneto-electronic devices expanded are based on magnetic semiconductor systems, where the magnetic ions like Mn, Cr, Co and Fe are introduced into non-magnetic semiconductors. In these magnetic semiconductors, a part of the lattice is made up of substitutional magnetic atoms. They are called diluted magnetic semiconductors (DMS). To employ spins in semiconductor, it is necessary to be able to generate, inject, transport, manipulate, and detect spins. In recent years there has been a wide research towards introducing ferromagnetic property such as spontaneous magnetization at room temperature in semiconductors to make new class of spintronic devices like spin valves, transistors, spin light emitting diodes, magnetic sensors, non-volatile memory, logic devices and ultra-fast switches. The potential advantages of spintronic devices will be higher speed, greater efficiency, and better stability, as well as low energy required to flip a spin.

1.3 Choice of materials

The major difficulty for practical application of spintronic devices is that efficient spin polarized carrier injection is required. Spin injection efficiency is often very low in conventional ferromagnetic metals due to resistivity differences and to the formation of Schottky barrier. A novel class of materials, dilute magnetic semiconductors (DMS), could be a best solution to this problem. The group II-VI semiconductors such as (Zn,Mn)Se or (Zn,Mn)S are examples of DMS. In DMS alloys the stoichiometric fraction of the constituent atoms is replaced by magnetic transition metals atoms to utilize the electrons spin in addition to its charge. These alloys are semiconductors and are able to process well defined magnetic properties such as paramagnetism, ferromagnetism and antiferromagnetism in compare with conventional semiconductors. DMS have been used to form magnetic and non-magnetic interfaces formed in heterostructures. It is been observed that incorporation of magnetic materials in these structures is a source of spin-polarized electrons. In addition the technological importance of group II-VI semiconductors make them a best choice for advanced research studies specially in the spintronic applications. The glass or ceramic substrates can be applied as substrate based on their special applications. Mostly used substrate is indium tin oxide. The most important factor to

facilitate nucleation and to avoid tension in growth of layers is the thermal expansion coefficient of substrate and grown layer should be similar.

1.4 Importance of the study

During the past decades, tremendous progress has made in basic units of the microelectronic industry. Devices continue to diminish in size in order to achieve higher speeds with less consumption of electricity. Several long-term alternative concepts are being investigated in order to attain the above matters by exploiting multifunctional properties of materials.

The theoretical understanding of semiconductor devices have developed rapidly since the first transistor was invented in 1949 (Kröger, 1978). Improved new technologies for growing semiconductor thin films of different structural and electronic properties have provided new opportunities for basic scientific studies and device applications. Current transistors operate much faster than conventional ones and have led many thousand-fold increases in speed, which is very crucial to the electronic and optical communication and computer industries. An increase in the speed of transistors has resulted from a reduction of charge transit time between terminals. Shorter charge transit time indicates minimum time delay of input signal to the output. Charge transit time has been shortened very efficiently by choosing semiconductor materials and device structures in which signals propagate faster by employing semiconductors with high electron mobility and velocity (Kang and Lee, 2013).

Over the past decade the experimental and theoretical study of quantum confinement of carriers in spatially modulated semiconductor structures has been an area of intense activity. Relatively new magnetic semiconductor quantum wells and superlattices have extended this field to include novel spin dependent phenomena. The purpose in spintronic devices is to use wide bandgap semiconductors such as ZnS and ZnSe which are suitable candidates to produce carrier-induced magnetism. A good knowledge about the mechanism of the magnetic interactions coupled with spins of the band carriers and localized spins of magnetic ions, could obtain which may result in different magnetic phases such as ferromagnetism, paramagnetism and antiferromagnetism (Xu and Thompson, 2006).

In this research 1D and 2D quantum structures are prepared using low cost electrodeposition method instead of expensive and sophisticated methods such as molecular beam epitaxy. The first part discussed the basic physics involved II-VI MS quantum structures. Clear and established underlying science and the relationship between structure and properties of these quantum structures are discussed. In addition more practical device from II-VI MS heterostructures is developed and showed spin injection and transport properties. The group II-VI MS alloy quantum structures are of interest that transition metal Mn^{2+} incorporated on the group II site of zinc blend lattice. Figure 1.1 shows the relation between lattice parameter and the energy band gap of some ternary alloys of II-VI magnetic semiconductors.

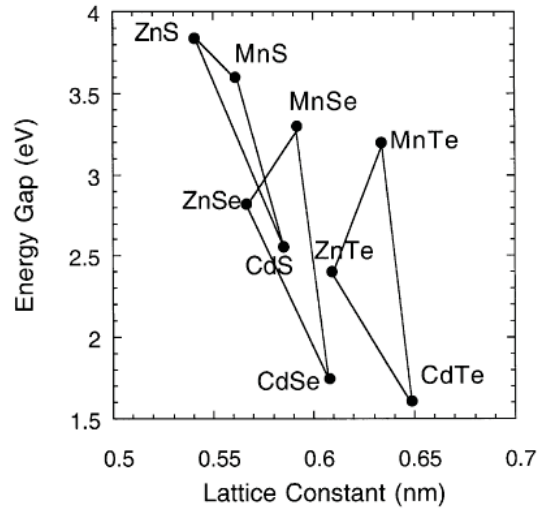


Figure 1.1: Summary of the energy gap at 4.2 K and lattice parameter of some II-VI MS alloys. The lines showing ternary alloys (Awschalom and Samarth, 1999).

There are different examples of ‘spin engineered’ MS heterostructures which are fabricated using sophisticated methods such as MBE. Here we only concentrate on the simplest MS heterostructures consist of binary non-magnetic quantum well flanked by MS barriers of ZnSe/(Zn,Mn)Se and ZnS/(Zn,Mn)S prepared by electrodeposition method.

In the second part we focused on semiconductor and magnetic semiconductor nanowires with different diameter prepared by electrodeposition method into polycarbonate membrane templates. The template assisted synthesis has recently proved to be a well-designed chemical approach for synthesis of nanoscale materials and an alternative to MBE method. There are a wide range of nanoporous materials. The most studies were performed using track-etched polymer membranes and anodic porous alumina membranes. Both membranes enable to make fibrils of uniform diameter in the range of nanometer. We will discuss the preparation method of NWs using polycarbonate (PCTE) membrane and presented morphological characterization dependent optical and electrical properties.

1.5 Problem statements

Nowadays, the most successful technologies are led by the data storage industries and the integrated circuits. Most of the current semiconductor devices use the charge of electrons and holes in order to perform their specific functionalities and ignore the spin of electrons. However the integrated circuits have advantages such as high speed and good reliability, but their memory elements are volatile which means that when the power is switched off the stored information is lost. Moreover, power dissipation and heat generation are becoming critical issues. On the other hand, the spin of electron is the key parameter in magnetic data storage technology and if we can harness the spin of the carriers within a material, the devices will show highly increased speed and storage density. Devices based on spin polarized can be used as

non-volatile memory because of the natural remanence characteristic of ferromagnetic materials without the need of the electrical power.

Fabrication of highly desirable heterostructures with homogeneous compounds, exactly controlled stoichiometry and atomically abrupt interfaces has been performed using advanced methods like molecular beam epitaxy. Unfortunately such methods are very expensive and many attempts have been performed to solve this problem. In this work our aim is to fabricate these heterostructures using simple and inexpensive method like electrodeposition. The valuable features of the electrodeposition method are its convenience in producing large area devices inexpensively and its low temperature growth which yields sharper junctions and control film thickness, morphology and composition by adjusting electrical parameters in an isothermal process.

The ability to achieve zincblende (Zn,Mn)Se having appreciable Mn content is crucial to quantum well studies, because a small variation in bandgap with Mn concentration make it necessary to grow barrier layers with a high Mn fraction to achieve sufficient band offset for carrier confinement.

1.6 Objectives of the study

The principal objective of this thesis is to synthesize and characterize low dimensional materials by low cost electrodeposition method, understand the basic science, particularly physics of the nanostructures and explore their technological applications. Thus the proposed research project has the following clear work-phase objectives.

1. To synthesize and optimize the deposition condition of ZnSe and ZnS thin films and characterize the structural dependent properties of 2D quantum structures.
2. To investigate the effect of manganese doping concentration on morphology, optical, electrical and magnetic properties.
3. To fabricate single quantum well heterostructures of ZnSe/(Zn,Mn)Se and ZnS/(Zn,Mn)S using electrodeposition method.
4. To demonstrate spin polarized injection using magnetic element as spin aligner and observe spin polarized transport effect.
5. To obtain ZnSe, ZnS, ZnSe-Mn and ZnS-Mn nanowires using template assisted method by electrodeposition and investigate the effect of pore diameter on their properties.

1.7 Outline of the thesis

Given the importance of detailed understanding of the structure, morphology and optical, electrical and magnetic properties of nanostructure materials for the application described above, this study will focus on the general introduction about the research background, problem statement and objectives of the study. Chapter 2 concerns with the review on background, synthesis and some characterization of low dimensional structures. Chapter 3 focused on theoretical background which includes brief introduction to spintronics, basic physics of thin film growth and heterostructures and fundamental of electrodeposition method. Chapter 4 highlights the methodology of the study; including materials, sample preparation and characterization methods applied. Chapter 5 deals with the results and discussion on characterization of single layer, three-layer thin films and nanowires. Chapter 6 summarizes the results and gives some suggestions for future work.

REFERENCES

- Aguilera-Sigalat, J., Bradshaw, D. (2015). Synthesis and applications of metal-organic framework–quantum dot (QD@ MOF) composites. *Coordination Chemistry Reviews*.
- Aichele, T., Tribu, A., Bougerol, C., Kheng, K., André, R., Tatarenko, S. (2008). Defect-free ZnSe nanowire and nanoneedle nanostructures. *Applied Physics Letters*, 93, 143106.
- Almasi-Kashi, M., Ramazani, A., Kheyri, F., Jafari-Khamse, E. (2014). The effect of magnetic layer thickness on magnetic properties of Fe/Cu multilayer nanowires. *Materials Chemistry and Physics*, 144, 230-234.
- Andorn, M., Bar-Eli, K. (1971). Optical Bleaching and Deviations from Beer—Lambert's Law of Solutions Illuminated by a Ruby Laser. I. Cryptocyanine Solutions. *The Journal of Chemical Physics*, 55, 5008-5017.
- Andrieux, C., Blocman, C., Dumas-Bouchiat, J., M'halla, F., Saveant, J. (1980). Homogeneous redox catalysis of electrochemical reactions: Part V. Cyclic voltammetry. *Journal of Electroanalytical Chemistry and Interfacial Electrochemistry*, 113, 19-40.
- Arbi, N., Assaker, I.B., Gannouni, M., Kriaa, A., Chtourou, R. (2015). Experimental investigation of the effect of Zn/S molar ratios on the physical and electrochemical properties of ZnS thin films. *Materials Science in Semiconductor Processing*, 40, 873-878.
- Arya, S., Khan, S., Lehana, P., Gupta, I., Kumar, S. (2014). Electrical properties of electrodeposited zinc selenide (ZnSe) nanowires. *Journal of Materials Science: Materials in Electronics*, 25, 4150-4155.
- Auerbach, S.M., Carrado, K.A., Dutta, P.K. 2003. Handbook of zeolite science and technology: CRC press.
- Awschalom, D., Samarth, N. (1999). Spin dynamics and quantum transport in magnetic semiconductor quantum structures. *Journal of magnetism and magnetic materials*, 200, 130-147.
- Bakiyaraj, G., Dhanasekaran, R. (2013). Synthesis and characterization of flower-like ZnSe nanostructured thin films by chemical bath deposition (CBD) method. *Applied Nanoscience*, 3, 125-131.
- Bantu, A.K.M., de Castro, A., de Magalhães, S., Barthem, V., Givord, D., de Miranda, P., Clemente, G., Simão, R. (2015). Structural and Magnetic Properties of Electrodeposited CoPt and FeCu Nanowires Embedded in Polycarbonate Membranes. *The African Review of Physics*, 9.

- Baset, S., Akbari, H., Zeynali, H., Shafie, M. (2011). Size measurement of metal and semiconductor nanoparticles via uv-vis absorption spectra. *Digest Journal of Nanomaterials & Biostructures (DJNB)*, 6.
- Bauer, G., Pascher, H., Zawadzki, W. (1992). Magneto-optical properties of semimagnetic lead chalcogenides. *Semiconductor science and technology*, 7, 703.
- Beck, J.S., Vartuli, J.C. (1996). Recent advances in the synthesis, characterization and applications of mesoporous molecular sieves. *Current Opinion in Solid State and Materials Science*, 1, 76-87.
- Belik, A.A., Kodama, K., Igawa, N., Shamoto, S.-i., Kosuda, K., Takayama-Muromachi, E. (2010). Crystal and magnetic structures and properties of $\text{BiMnO}_3 + \delta$. *Journal of the American Chemical Society*, 132, 8137-8144.
- Belov, N.A., Aksenov, A.A., Eskin, D.G. 2002. Iron in aluminium alloys: impurity and alloying element: *CRC Press*.
- Bimberg, D., Grundmann, M., Ledentsov, N.N. 1999. Quantum dot heterostructures: *John Wiley & Sons*.
- Blondel, A., Meier, J., Doudin, B., Ansermet, J.-P., Attenborough, K., Evans, P., Hart, R., Nabiyouni, G., Schwarzacher, W. (1995). Wire-shaped magnetic multilayers for 'current perpendicular to plane' magnetoresistance measurements. *Journal of magnetism and magnetic materials*, 148, 317-318.
- Bockris, J.M. (1956). Kinetics of activation controlled consecutive electrochemical reactions: anodic evolution of oxygen. *The Journal of Chemical Physics*, 24, 817-827.
- Brylev, O., Roué, L., Bélanger, D. (2005). Rhodium electrodeposition on pyrolytic graphite electrode: Analysis of chronoamperometric curves. *Journal of Electroanalytical Chemistry*, 581, 22-30.
- Bu, L.-X., Wang, W. (2007). *Studies on the electrodeposition behavior of selenium by electrochemical impedance spectroscopy and cyclic voltammetry*. Paper presented at the Thermoelectrics, 2007. ICT 2007. 26th International Conference on.
- Burkard, G. (2008). Quantum information: Positively spin coherent. *Nature materials*, 7, 100-101.
- Chandramohan, R., Mahalingam, T., Chu, J., Sebastian, P. (2005). Preparation and characterization of electrosynthesized zinc selenide thin films. *Journal of New Materials for Electrochemical Systems*, 8, 143-148.
- Chang, T., Cho, S., Kim, J., Schoenleber, J., Frantz, C., Stein, N., Boulanger, C., Lee, W. (2015). Individual thermoelectric properties of electrodeposited

bismuth telluride nanowires in polycarbonate membranes. *Electrochimica Acta*, 161, 403-407.

Chen, L., Zhang, D., Zhai, G., Zhang, J. (2010). Comparative study of ZnSe thin films deposited from modified chemical bath solutions with ammonia-containing and ammonia-free precursors. *Materials Chemistry and Physics*, 120, 456-460.

Chen, S., Slattum, P., Wang, C., Zang, L. (2015a). Self-Assembly of Perylene Imide Molecules into 1D Nanostructures: Methods, Morphologies, and Applications. *Chemical reviews*, 115, 11967-11998.

Chen, X., Mao, S.S. (2007). Titanium dioxide nanomaterials: synthesis, properties, modifications, and applications. *Chemical reviews*, 107, 2891-2959.

Chen, Y., Cui, X., Yao, X. (2015b). Peritectic melting of thin films, superheating and applications in growth of REBCO superconductors. *Progress in Materials Science*, 68, 97-159.

Chen, Y., Duan, J., Yao, H., Mo, D., Liu, T., Wang, T., Hou, M., Sun, Y., Liu, J. (2014). Facile preparation and magnetic properties of Ni nanotubes in polycarbonate ion-track templates. *Physica B: Condensed Matter*, 441, 1-5.

Colletti, L.P., Flowers, B.H., Stickney, J.L. (1998). Formation of thin films of CdTe, CdSe, and CdS by electrochemical atomic layer epitaxy. *Journal of the Electrochemical Society*, 145, 1442-1449.

Cortés, M., Gómez, E., Vallés, E. (2013). Electrochemical growth of CoPt nanowires of different aspect ratio and their magnetic properties. *Journal of Electroanalytical Chemistry*, 689, 69-75.

Crowell, P. (2015). Spin Accumulation and its Detection in Ferromagnet/III-V Semiconductor Devices. *Bulletin of the American Physical Society*, 60.

Cruz-Acuña, M., Bailón-Ruiz, S., Marti-Figueroa, C.R., Cruz-Acuña, R., Perales-Pérez, O.J. (2015). Synthesis, characterization and evaluation of the cytotoxicity of Ni-doped Zn (Se, S) quantum dots. *Journal of Nanomaterials*, 2015, 49.

Dasgupta, N.P., Sun, J., Liu, C., Brittman, S., Andrews, S.C., Lim, J., Gao, H., Yan, R., Yang, P. (2014). 25th anniversary article: semiconductor nanowires—synthesis, characterization, and applications. *Advanced Materials*, 26, 2137-2184.

de Moraes, A., Mosca, D., Schreiner, W., Mattoso, N., Silveira, E. (2002). Structural and chemical properties of ZnSe-Fe electrodeposited granular films. *Brazilian journal of physics*, 32, 383-385.

- Dietl, T., Ohno, H., Matsukura, F., Cibert, J., Ferrand, D. (2000). Zener model description of ferromagnetism in zinc-blende magnetic semiconductors. *Science*, 287, 1019-1022.
- Dong, G.-H., Zhu, Y.-J., Cheng, G.-F., Ruan, Y.-J. (2012). Cu (2– X) Te nanowires synthesized by a microwave-assisted solvothermal method using a self-sacrificial template and their electrical conductivity. *Materials Letters*, 76, 69-72.
- Eaton, C., Moyer, J.A., Alipour, H.M., Grimley, E.D., Brahlek, M., LeBeau, J.M., Engel-Herbert, R. (2015). Growth of SrVO₃ thin films by hybrid molecular beam epitaxy. *Journal of Vacuum Science & Technology A*, 33, 061504.
- Eaton, G.R., Eaton, S.S., Salikhov, K.M. 1998. Foundations of modern EPR: *World Scientific*.
- Echendu, O., Weerasinghe, A., Diso, D., Fauzi, F., Dharmadasa, I. (2013). Characterization of n-Type and p-Type ZnS thin layers grown by an electrochemical method. *Journal of electronic materials*, 42, 692-700.
- Echendu, O.K., Dharmadasa, I.M. (2015). Graded-bandgap solar cells using all-electrodeposited ZnS, CdS and CdTe thin-films. *Energies*, 8, 4416-4435.
- Elliot, T.B. 2005. Trends in Semiconductor Research: *Nova Publishers*.
- Esaki, L. (1988). A bird's-eye view on the evolution of semiconductor superlattices and quantum wells *Electronic Structure of Semiconductor Heterojunctions (pp. 56-69): Springer*.
- Esteves, A.C.C., Trindade, T. (2002). Synthetic studies on II/VI semiconductor quantum dots. *Current Opinion in Solid State and Materials Science*, 6, 347-353.
- Farrow, R.F., Parkin, S., Dobson, P., Neave, J., Arrott, A. 2013. Thin film growth techniques for low-dimensional structures (Vol. 163): *Springer Science & Business Media*.
- Fert, A., Piraux, L. (1999). Magnetic nanowires. *Journal of Magnetism and Magnetic Materials*, 200, 338-358.
- Fewster, P.F. (1996). X-ray analysis of thin films and multilayers. *Reports on Progress in Physics*, 59, 1339.
- Fiederling, R., Keim, M., Reuscher, G.a., Ossau, W., Schmidt, G., Waag, A., Molenkamp, L. (1999). Injection and detection of a spin-polarized current in a light-emitting diode. *Nature*, 402, 787-790.
- Fukumura, H., Irie, M., Iwasawa, Y., Masuhara, H., Uosaki, K. 2009. Molecular nano dynamics: *John Wiley & Sons*.

- Furdyna, J.K. (1988). Diluted magnetic semiconductors. *Journal of Applied Physics*, 64, R29-R64.
- Gao, F., Liu, Y., Fan, Y., Zhao, D. (2016). Synthesis of N-acetyl-L-cysteine-capped ZnCdSe quantum dots via hydrothermal method and their characterization. *Science and Technology of Advanced Materials*.
- Gfroerer, T.H. (2000). Photoluminescence in analysis of surfaces and interfaces. *Encyclopedia of Analytical Chemistry*.
- Giebultowicz, T., Rhyne, J., Furdyna, J. (1987). Mn-Mn exchange constants in zinc-manganese chalcogenides. *Journal of Applied Physics*, 61, 3537-3539.
- Gielisse, P. 1998. Diamond and diamond-like film applications: *CRC Press*.
- Goddard III, W.A., Brenner, D., Lyshevski, S.E., Iafrate, G.J. 2007. Handbook of nanoscience, engineering, and technology: *CRC press*.
- Goede, O., Heimbrodt, W., Hieke, K., Gumlich, H.-E., Pier, T., Lunn, B., Ashenford, D., Jackson, S., Nicholls, J. (1992). Exciton transfer in CdTe (Cd, Mn) Te-double quantum well structures. *Superlattices and microstructures*, 12, 363-366.
- Goswami, A. 1996. Thin film fundamentals: *New Age International*.
- Gubicza, J. 2014. X-ray line profile analysis in materials science: *IGI Global*.
- Guichard, P.J.Y., Derennes, C. (2015). Method for Producing a Semiconducting Organic Film: *US Patent 20,150,372,232*.
- Gupta, M.C., Ballato, J. 2006. The handbook of photonics: *CRC press*.
- Hammond, C., Hammond, C. 2009. The basics of crystallography and diffraction: *Oxford University Press Oxford*.
- Hanif, K.M., Meulenberg, R.W., Strouse, G.F. (2002). Magnetic ordering in doped Cd_{1-x}Co_xSe diluted magnetic quantum dots. *Journal of the American Chemical Society*, 124, 11495-11502.
- Harrison, P. 2005. Quantum wells, wires and dots: theoretical and computational physics of semiconductor nanostructures: *John Wiley & Sons*.
- Henini, M. 2012. Molecular beam epitaxy: from research to mass production: *Newnes*.
- Hennayaka, H., Lee, H.S. (2013). Structural and optical properties of ZnS thin film grown by pulsed electrodeposition. *Thin Solid Films*, 548, 86-90.
- Herman, M., Jylhä, O., Pessa, M. (1984). Atomic layer epitaxy of Cd_{1-x}Mn_xTe grown on CdTe (111) B substrates. *Journal of crystal growth*, 66, 480-483.

- Hernández-Rodríguez, I., García, J.M., Martín-Gago, J.A., de Andrés, P.L., Méndez, J. (2015). Graphene growth on Pt (111) and Au (111) using a MBE carbon solid-source. *Diamond and Related Materials*.
- Huang, L., Lu, J.G. (2015). Synthesis, Characterizations and Applications of Cadmium Chalcogenide Nanowires: A Review. *Journal of Materials Science & Technology*, 31, 556-572.
- Huang, Q. 2008. Size and surface effects on the electrical properties of metallic nanowires: *ProQuest*.
- Huang, Z. (2015). *Towards Room-Temperature deterministic ferroelectric control of ferromagnetic thin films*. ÉCOLE POLYTECHNIQUE FÉDÉRALE DE LAUSANNE.
- Idza, I., Hashim, M., Rodziah, N., Ismayadi, I., Norailiana, A. (2012). Influence of evolving microstructure on magnetic-hysteresis characteristics in polycrystalline nickel-zinc ferrite, Ni_{0.3}Zn_{0.7}Fe₂O₄. *Materials Research Bulletin*, 47, 1345-1352.
- Jang, B., Pellicer, E., Guerrero, M., Chen, X., Choi, H., Nelson, B.J., Sort, J., Pané, S. (2014). Fabrication of Segmented Au/Co/Au Nanowires: Insights in the Quality of Co/Au Junctions. *ACS applied materials & interfaces*, 6, 14583-14589.
- Jankowski, S., Heimbrodt, W. (2010). Energy transfer in ZnSe/(Zn, Mn) Se double quantum wells. *physica status solidi (c)*, 7, 1639-1641.
- Jeyachitra, R., Senthilnathan, V., Kathirvel, D. Optical, Photoluminescence and Electrical properties of Vacuum evaporated ZnS thin films.
- Kaeslin, H. 2008. Digital integrated circuit design: from VLSI architectures to CMOS fabrication: *Cambridge University Press*.
- Kang, S., Lee, K. (2013). Emerging materials and devices in spintronic integrated circuits for energy-smart mobile computing and connectivity. *Acta Materialia*, 61, 952-973.
- Kasap, S., Capper, P. 2006. Springer handbook of electronic and photonic materials: *Springer Science & Business Media*.
- Kassim, A., Nagalingam, S., Min, H.S., Karrim, N. (2010). XRD and AFM studies of ZnS thin films produced by electrodeposition method. *Arabian Journal of Chemistry*, 3, 243-249.
- Kassim, A., Tan, W.T., Ho, S.M., Nagalingam, S. (2011). Composition, morphology and optical characterization of chemical bath deposited ZnSe thin films. *European Journal of Applied Science*, 3, 75-80.

- Kharisov, B.I., Kharissova, O.V., Méndez, U.O. 2013. Radiation Synthesis of Materials and Compounds: *CRC Press*.
- Kim, C., Kim, M., Lee, S., Kossut, J., Furdyna, J., Dobrowolska, M. (2000). CdSe quantum dots in a Zn $1-x$ Mn x Se matrix: new effects due to the presence of Mn. *Journal of crystal growth*, 214, 395-399.
- Kim, Y., Jung, J., Kim, S., Chae, W.-S. (2013). Cyclic Voltammetric and Chronoamperometric Deposition of CdS. *Materials Transactions*, 54, 1467-1472.
- Kissinger, P.T., Heineman, W.R. (1983). Cyclic voltammetry. *J. Chem. Educ*, 60, 702.
- Kittel, C. 2005. Introduction to solid state physics: *Wiley*.
- Klockenkämper, R., von Bohlen, A. 2014. Total-Reflection X-Ray Fluorescence Analysis and Related Methods: *John Wiley & Sons*.
- Kole, A.K., Kumbhakar, P. (2012). Cubic-to-hexagonal phase transition and optical properties of chemically synthesized ZnS nanocrystals. *Results in Physics*, 2, 150-155.
- Kröger, F. (1978). Cathodic deposition and characterization of metallic or semiconducting binary alloys or compounds. *Journal of The Electrochemical Society*, 125, 2028-2034.
- Kuech, T. 2014. Handbook of Crystal Growth: Thin Films and Epitaxy: *Elsevier*.
- Kumar, A.A. 2008. Pulse and Digital Circuits: *PHI Learning Pvt. Ltd.*
- Kumar, S., Vohra, A., Chakarvarti, S. (2012a). Electrical properties of electrodeposited ZnCuTe ternary nanowires embedded in polycarbonate membrane. *Nanomaterials and Nanotechnology*, 2, 2-3.
- Kumar, V., Sengupta, S., Raj, B. 2012b. Frontiers in Materials Modelling and Design: Proceedings of the Conference on Frontiers in Materials Modelling and Design, Kalpakkam, 20–23 August 1996: *Springer Science & Business Media*.
- Kumaresan, R., Ichimura, M., Arai, E. (2002). Photochemical deposition of ZnSe polycrystalline thin films and their characterization. *Thin solid films*, 414, 25-30.
- Lad, A.D., Rajesh, C., Khan, M., Ali, N., Gopalakrishnan, I., Kulshreshtha, S., Mahamuni, S. (2007). Magnetic behavior of manganese-doped ZnSe quantum dots. *Journal of applied physics*, 101, 103906.
- Law, M., Goldberger, J., Yang, P. (2004). Semiconductor nanowires and nanotubes. *Annu. Rev. Mater. Res.*, 34, 83-122.

- Li, H., Wu, J., Wang, Z.M. 2013. Silicon-based nanomaterials: *Springer*.
- Li, Y., Yang, X.-Y., Feng, Y., Yuan, Z.-Y., Su, B.-L. (2012). One-dimensional metal oxide nanotubes, nanowires, nanoribbons, and nanorods: synthesis, characterizations, properties and applications. *Critical Reviews in Solid State and Materials Sciences*, 37, 1-74.
- Lim, E.C. 2013. Excited states (Vol. 4): *Elsevier*.
- Lincot, D. (2005). Electrodeposition of semiconductors. *Thin Solid Films*, 487, 40-48.
- Liu, H., Zhang, H., Liu, D. (2015). Spin transport and tunnel magnetoresistance in ferromagnetic graphene/Thue–Morse graphene superlattice double junction. *Physics Letters A*, 379, 192-198.
- Liu, J., Ma, J., Liu, Y., Song, Z., Sun, Y., Fang, J., Liu, Z. (2009). Synthesis of ZnS nanoparticles via hydrothermal process assisted by microemulsion technique. *Journal of Alloys and Compounds*, 486, L40-L43.
- Liu, W.K., Santos, M.B. 1999. Thin films: Heteroepitaxial systems (Vol. 15): *World Scientific*.
- Liu, Z., El Abedin, S.Z., Ghazvini, M., Endres, F. (2013). Electrochemical synthesis of vertically aligned zinc nanowires using track-etched polycarbonate membranes as templates. *Physical Chemistry Chemical Physics*, 15, 11362-11367.
- Llavona, Á., Pérez, L., Sánchez, M.C., de Manuel, V. (2013). Enhancement of anomalous codeposition in the synthesis of Fe–Ni alloys in nanopores. *Electrochimica Acta*, 106, 392-397.
- Lü, X., Yang, J., Fu, Y., Liu, Q., Qi, B., Lü, C., Su, Z. (2010). White light emission from Mn²⁺ doped ZnS nanocrystals through the surface chelating of 8-hydroxyquinoline-5-sulfonic acid. *Nanotechnology*, 21, 115702.
- Mackay, D.T., Janish, M.T., Sahaym, U., Kotula, P.G., Jungjohann, K.L., Carter, C.B., Norton, M.G. (2014). Template-free electrochemical synthesis of tin nanostructures. *Journal of Materials Science*, 49, 1476-1483.
- Maekawa, S., Shinjo, T. 2002. Spin dependent transport in magnetic nanostructures: *CRC Press*.
- Mahalingam, T., Kathalingam, A., Lee, S., Moon, S., Kim, Y.D. (2007). Studies of electrosynthesized Zinc Selenide thin films. *Journal of New Materials for Electrochemical Systems*, 10, 15.
- Mahalingam, T., Kathalingam, A., Velumani, S., Lee, S., Sun, M., Deak, K. (2006). Electrochemical synthesis and characterization of zinc selenide thin films. *Journal of materials science*, 41, 3553-3559.

- Mahalingam, T., Thanikaikarasan, S., Dhanasekaran, V., Kathalingam, A., Velumani, S., Rhee, J.-K. (2010). Preparation and characterization of MnSe thin films. *Materials Science and Engineering: B*, 174, 257-262.
- Mane, R., Lokhande, C. (2000). Chemical deposition method for metal chalcogenide thin films. *Materials Chemistry and Physics*, 65, 1-31.
- Manzoli, A., Santos, M., Machado, S. (2007). A voltammetric and nanogravimetric study of ZnSe electrodeposition from an acid bath containing Zn (II) and Se (IV). *Thin Solid Films*, 515, 6860-6866.
- Misiuna, P., Dłużewski, P., Wojciechowski, T., Milińska, E., Kurowska, B., Wiater, M., Wawro, A., Wojtowicz, T., Baczewski, L. (2015). Structural and magnetic properties of hybrid ferromagnetic metal/semiconductor (ZnTe)/Co core-shell nanowires. *Journal of Crystal Growth*, 412, 80-86.
- Moore, G., Read, N. (1991). Nonabelions in the fractional quantum Hall effect. *Nuclear Physics B*, 360, 362-396.
- Murali, K. (2014). Optical properties of pulse electrodeposited ZnS films. *IOSR Journal of Applied Physics*, 6, 9.
- Murugadoss, G. (2011). Synthesis, optical, structural and thermal characterization of Mn²⁺ doped ZnS nanoparticles using reverse micelle method. *Journal of Luminescence*, 131, 2216-2223.
- Nabiyouni, G., Sahraei, R., Toghiani, M., Ara, M.M., Hedayati, K. (2011). Preparation and characterization of nano-structured zns thin films grown on glass and n-type si substrates using a new chemical bath deposition technique. *Rev. Adv. Mater. Sci*, 27, 52-57.
- Nalwa, H.S. 1999. Handbook of Nanostructured Materials and Nanotechnology, Five-Volume Set (Vol. 3): *Academic Press*.
- Nalwa, H.S. 2001. Handbook of surfaces and interfaces of materials, five-volume set: *Academic press*.
- Nasr, A.B., Habchi, M., Bilel, C., Rebey, A., El Jani, B. (2015). Theoretical calculations of absorption spectra of GaNAsBi-based MQWs operating at 1.55 μm . *Journal of Alloys and Compounds*, 647, 159-166.
- Ndukwe, I. (1996). Solution growth, characterization and applications of zinc sulphide thin films. *Solar energy materials and solar cells*, 40, 123-131.
- Olusola, O., Madugu, M., Abdul-Manaf, N., Dharmadasa, I. (2016). Growth and characterisation of n-and p-type ZnTe thin films for applications in electronic devices. *Current Applied Physics*, 16, 120-130.

- Oppo, G.-L., Barnett, S.M., Riis, E., Wilkinson, M. 1997. Quantum Dynamics of Simple Systems: Proceedings of the Forty Fourth Scottish Universities Summer School in Physics, Stirling, August 1994 (Vol. 44): CRC Press.
- Owen, J.I. 2011. Growth, Etching, and Stability of Sputtered ZnO: Al for Thin-Film Silicon Solar Cells (Vol. 125): Forschungszentrum Jülich.
- Owens, F.J. 2015. Physics of Magnetic Nanostructures: John Wiley & Sons.
- Ozmetin, A., Ongun, E., Kuru, M., Yazici, E. (2015). Fabrication and characterization of ferromagnetic–superconducting hybrid films grown by combined PVD techniques. *Applied Surface Science*, 350, 2-5.
- Ozutok, F., Erturk, K., Bilgin, V. (2012). Growth, Electrical, and Optical Study of ZnS: Mn Thin Films. *Acta Physica Polonica-Series A General Physics*, 121, 221.
- Panda, S.K., Hickey, S.G., Demir, H.V., Eychmüller, A. (2011). Bright White-Light Emitting Manganese and Copper Co-Doped ZnSe Quantum Dots. *Angewandte Chemie*, 123, 4524-4528.
- Park, K., Krivoy, E., Nair, H., Bank, S., Yu, E. (2015). Cross-sectional scanning thermal microscopy of ErAs/GaAs superlattices grown by molecular beam epitaxy. *Nanotechnology*, 26, 265701.
- Paul, S. (2015). Studies on the effect of defects and dopants on the optical photocatalytic and magnetic properties of tio2 nanoparticles.
- Pawar, S., Pawar, B., Kim, J., Joo, O.-S., Lokhande, C. (2011). Recent status of chemical bath deposited metal chalcogenide and metal oxide thin films. *Current Applied Physics*, 11, 117-161.
- Pelekanos, N., Ding, J., Hagerott, M., Nurmikko, A., Luo, H., Samarth, N., Furdyna, J. (1992). Quasi-two-dimensional excitons in (Zn, Cd) Se/ZnSe quantum wells: Reduced exciton–LO-phonon coupling due to confinement effects. *Physical Review B*, 45, 6037.
- Penc, K., Hallberg, K., Mila, F., Shiba, H. (1996). Shadow band in the one-dimensional infinite-U Hubbard model. *Physical review letters*, 77, 1390.
- Philipose, U., Sun, P., Xu, T., Ruda, H.E., Yang, L., Kavanagh, K. (2007). Structure and photoluminescence of ZnSe nanostructures fabricated by vapor phase growth. *Journal of applied physics*, 101, 014326.
- Poornaprakash, B., Sambasivam, S., Reddy, D.A., Murali, G., Vijayalakshmi, R., Reddy, B. (2014). Dopant induced RTFM and enhancement of fluorescence efficiencies in spintronic ZnS: Ni nanoparticles. *Ceramics International*, 40, 2677-2684.

- Pullar, R.C. (2012). Hexagonal ferrites: a review of the synthesis, properties and applications of hexaferrite ceramics. *Progress in Materials Science*, 57, 1191-1334.
- Pung, S., Choy, K. (2016). Aluminium-Doped ZnO Films and Nanowires by a Modified Chemical Vapor Deposition Technique. *une*, 13, 15.
- Rajeshwar, K., de Tacconi, N.R. (1997). Electrodeposition and characterization of nanocrystalline semiconductor films. *Studies in Surface Science and Catalysis*, 103, 321-351.
- Ramirez, A., Cava, R., Krajewski, J. (1997). Colossal magnetoresistance in Cr-based chalcogenide spinels.
- Rao, C., Deepak, F., Gundiah, G., Govindaraj, A. (2003). Inorganic nanowires. *Progress in Solid State Chemistry*, 31, 5-147.
- Richards, R.D., Bastiman, F., Roberts, J.S., Beanland, R., Walker, D., David, J.P. (2015). MBE grown GaAsBi/GaAs multiple quantum well structures: Structural and optical characterization. *Journal of Crystal Growth*.
- Riveros, G., Gomez, H., Henriquez, R., Schrebler, R., Marotti, R., Dalchiele, E. (2001). Electrodeposition and characterization of ZnSe semiconductor thin films. *Solar energy materials and solar cells*, 70, 255-268.
- Sadao, A. (2005). Properties of Group-IV, III-V and II-VI Semiconductors. *England: John Wiley & Sons Ltd*373.
- Saito, C., Kato, H., Sano, M. (2015). Method for producing p-type ZnO based compound semiconductor layer, method for producing ZnO based compound semiconductor element, and an n-type ZnO based compound semiconductor laminate structure: *Google Patents*.
- Samantilleke, A., Boyle, M., Young, J., Dharmadasa, I. (1998). Growth of n-type and p-type ZnSe thin films using an electrochemical technique for applications in large area optoelectronic devices. *Journal of Materials Science: materials in electronics*, 9, 231-235.
- Sanderson, R. 2012. Chemical Bonds and Bonds Energy (Vol. 21): *Elsevier*.
- Schlesinger, M., Paunovic, M. 2011. Modern electroplating (Vol. 55): *John Wiley & Sons*.
- Schmitt-Rink, S., Chemla, D., Miller, D. (1989). Linear and nonlinear optical properties of semiconductor quantum wells. *Advances in Physics*, 38, 89-188.
- Semenov, N.N. 2013. Some problems of chemical kinetics and reactivity (Vol. 1): *Elsevier*.

- Sen, A.K., Bardhan, K.K., Chakrabarti, B.K. 2009. Quantum and semi-classical percolation and breakdown in disordered solids (*Vol. 762*): Springer.
- Seo, K.W., Lee, S.S., Park, J.P., Shim, I. (2006). Single-source precursor based ZnSe thin film preparation through MOCVD method. *Bulletin-Korean Chemical Society*, 27, 2074.
- Seshan, K. 2012. Handbook of thin film deposition: *William Andrew*.
- Shah, A., Ahmad, J., Ahmad, I., Mehmood, M., Mahmood, A., Rasheed, M.A. (2014). Copper ion implanted aluminum nitride dilute magnetic semiconductors (DMS) prepared by molecular beam epitaxy. *Applied Surface Science*, 317, 262-268.
- Singh, R., Bhushan, S., Singh, A., Deo, S. (2011). Characterization and optical properties of CdSe nano-crystalline thin films. *Digest Journal of Nanomaterials and Biostructures*, 6, 403-412.
- Singh, S.C., Zeng, H., Guo, C., Cai, W. 2012. Nanomaterials: processing and characterization with lasers: *John Wiley & Sons*.
- Sirkeli, V.P., Nedeoglo, D.D., Nedeoglo, N.D., Radevici, I.V., Sobolevskaia, R.L., Sushkevich, K.D., Lähderanta, E., Lashkul, A.V., Laiho, R., *et al.* (2012). Magnetic and luminescent properties of manganese-doped ZnSe crystals. *Physica B: Condensed Matter*, 407, 3802-3807.
- Skjeltorp, A., Sherrington, D. 2012. Dynamical properties of unconventional magnetic systems (*Vol. 349*): *Springer Science & Business Media*.
- Solanki, R., Huo, J., Freeouf, J., Miner, B. (2002). Atomic layer deposition of ZnSe/CdSe superlattice nanowires. *Applied physics letters*, 81, 3864-3866.
- Song, J., Kulinich, S.A., Yan, J., Li, Z., He, J., Kan, C., Zeng, H. (2013). Epitaxial ZnO Nanowire-on-Nanoplate Structures as Efficient and Transferable Field Emitters. *Advanced Materials*, 25, 5750-5755.
- Song, S., Bohuslav, G., Capitano, A., Du, J., Taniguchi, K., Cai, Z., Sun, L. (2012). Experimental characterization of electrochemical synthesized Fe nanowires for biomedical applications. *Journal of Applied Physics*, 111, 056103.
- Stone, M. 1992. Quantum Hall Effect: *World Scientific*.
- Takemura, Y., Nakanishi, H., Konagai, M., Takahashi, K. (1991). Self-limiting growth in atomic layer epitaxy of ZnTe. *Japanese journal of applied physics*, 30, L246.
- Tiabl'kov, S.V. 2013. Methods in the quantum theory of magnetism: *Springer*.
- Tilley, R.J. 2004. Understanding solids: the science of materials: *John Wiley & Sons*.

- Trache, A., Meininger, G.A. (2008). Atomic force microscopy (AFM). *Current protocols in microbiology* 2C. 2.1-2C. 2.17.
- Valizadeh, S., George, J., Leisner, P., Hultman, L. (2002). Electrochemical synthesis of Ag/Co multilayered nanowires in porous polycarbonate membranes. *Thin Solid Films*, 402, 262-271.
- Van de Walle, C.G. 2012. Wide-band-gap Semiconductors: *Elsevier*.
- Venkatachalam, S., Mangalaraj, D., Narayandass, S.K., Kim, K., Yi, J. (2005). Structure, optical and electrical properties of ZnSe thin films. *Physica B: Condensed Matter*, 358, 27-35.
- Vilarinho, P. (2005). Functional materials: Properties, processing and applications *Scanning Probe Microscopy: Characterization, Nanofabrication and Device Application of Functional Materials (pp. 3-33): Springer*.
- Vopsaroiu, M., Blackburn, J., Cain, M.G. (2007). A new magnetic recording read head technology based on the magneto-electric effect. *Journal of Physics D: Applied Physics*, 40, 5027.
- Wang, K., Wu, H., Meng, Y., Wei, Z. (2014). Conducting polymer nanowire arrays for high performance supercapacitors. *Small*, 10, 14-31.
- Warren, E.L., Kibbler, A.E., France, R.M., Norman, A.G., Stradins, P., McMahon, W.E. (2015). Growth of antiphase-domain-free GaP on Si substrates by metalorganic chemical vapor deposition using an in situ AsH₃ surface preparation. *Applied Physics Letters*, 107, 082109.
- Wendt, H., Kreysa, G. 1999. Electrochemical engineering: science and technology in chemical and other industries: *Springer Science & Business Media*.
- Wertz, J. 2012. Electron spin resonance: elementary theory and practical applications: *Springer Science & Business Media*.
- Wu, M., Xiong, Y., Jiang, N., Ning, M., Chen, Q. (2004). Hydrothermal preparation of α -MnSe and MnSe 2 nanorods. *Journal of crystal growth*, 262, 567-571.
- Xia, J., Ge, W., Chang, K. 2012. Semiconductor spintronics: *World Scientific*.
- Xu, X.-J., Fei, G.-T., Yu, W.-H., Wang, X.-W., Chen, L., Zhang, L.-D. (2005). Preparation and formation mechanism of ZnS semiconductor nanowires made by the electrochemical deposition method. *Nanotechnology*, 17, 426.
- Xu, Y., Thompson, S. 2006. Spintronic materials and technology: *CRC Press*.
- Xu, Y., Wong, J., Liu, W., Niu, D., Zhang, W., Lu, Y., Hassan, S., Yan, Y., Will, I. (2016). Magnetic/III-V Semiconductor Based Hybrid Structures. *Handbook of Spintronics* 285-333.

- Xuan, T.-T., Liu, J.-Q., Xie, R.-J., Li, H.-L., Sun, Z. (2015). Microwave-assisted synthesis of CdS/ZnS: Cu quantum dots for white light-emitting diodes with high color rendition. *Chemistry of Materials*, 27, 1187-1193.
- Yoshida, T., Terada, K., Schlettwein, D., Oekermann, T., Sugiura, T., Minoura, H. (2000). Electrochemical Self-Assembly of Nanoporous ZnO/Eosin Y Thin Films and Their Sensitized Photoelectrochemical Performance. *Advanced Materials*, 12, 1214-1217.
- Zhang, Y. (2012). Controllable Synthesis, Structure and Property Modulation and Device Application of One-Dimensional Nanomaterials-Proceedings of the 4th International Conference on One-Dimensional Nanomaterials (ICON2011). *Circuits Systems and Signal Processing*, 1.
- Zhao, Y., Zhao, H., Liu, C., Cai, Z., Wang, J., Fu, X. (2015). Cathodic deposition of copper on polyaniline-coated textiles from a citrate bath: effects of electroplating conditions. *Journal of Materials Science: Materials in Electronics*, 26, 3621-3628.
- Zhu, L., Susac, D., Lam, A., Teo, M., Wong, P., Bizzotto, D., Campbell, S., Parsons, R., Mitchell, K. (2006). Structure of sputtered Co–Se thin films prepared for an application in catalysis. *Journal of Solid State Chemistry*, 179, 3942-3948.